COMBINED HYDROLOGY AND SLOPE STABILITY

ASSESSMENT OF THE OLYMPIC REGION

OF WASHINGTON STATE

By

CRAIG ABRAM JORDAN

A thesis submitted in partial fulfillment of
the requirements for the degree of

MASTER OF SCIENCE IN CIVIL ENGINEERING

WASHINGTON STATE UNIVERSITY
Department of Civil and Environmental Engineering

AUGUST 2011

To the Faculty of Washington State University

The members of the Committee appointed to examine the thesis of CRAIG ABRAM JORDAN find it satisfactory and recommend that it be accepted.

_____
Balasingam Muhunthan, Ph.D., Chair

_____
Jennifer Adam, Ph.D.

_____
William Cofer, Ph.D.

ACKNOWLEDGEMENT

COMBINED HYDROLOGY AND SLOPE STABILITY

ASSESSMENT OF THE OLYMPIC REGION

OF WASHINGTON STATE

Abstract

by Craig Abram Jordan, M.S.
Washington State University

Chair: Balasingam Muhunthan

Landslides constitute a major geological hazard in the world due to their high financial cost and their nondiscriminatory nature. The Olympic Region of Washington State has many potential triggers of landslides, but prolonged periods of high rainfall is the most commonly attributed trigger of landslides.

The current state of practice for landslide prediction is to assume pore water pressure above the phreatic surface is negligible; this methodology is incapable of accurately forecasting shallow landslides where suction plays a critical role. Suction varies with moisture content and as such a hydrological model that can be prescribed with varying vegetation and climate realizations should be used along with a stability model that includes soil suction to better predict shallow landslides.

This study presents a methodology to predict the stability of shallow planar slope failures that incorporates the hydrologic modeling capabilities of the program

iv

Combined/Hydrology And Slope Stability (CHASM). An infinite limit equilibrium stability model that includes the effects of soil suction is developed for this purpose. The hydrologic model predicts the water conditions above and below the phreatic surface while the incorporation of soil suction more accurately predicts the shear strength of the soil above the phreatic surface.

The methodology was shown to be effective in predicting slope failures above the phreatic surface during two simulations that were carried out for the Olympic Region (Queets River Slope and Clallam Slope). Utilizing rainfall data from the December 2007 storm event, failure was predicted above the phreatic surface around the 24th hour since rainfall for the Queets River Slope and around the 74th hour for the Clallam River Slope. Finally, design charts were developed for determination of the critical rainfall event for given slope angles and vegetative covers. The design charts predict failure in a 60 degree Hyas Gravelly Loam slope immediately after timber harvest if rainfall reaches 67-milimeters (2.6-inches) in a 24 hour period. These charts are intended for use by both engineers and land management personnel to manage and predict slope failures in the timber harvested Olympic Region of Washington State.

TABLE OF CONTENTS

LIST OF TABLES

LIST OF FIGURES

CHAPTER 1

INTRODUCTION

1.1 Background

Often overlooked in comparison to other geological hazards in the United States, such as earthquakes, volcanic eruptions, or tsunamis, landslides constitute a major geological hazard because they are widespread, occurring in all 50 states, and are estimated to cause $1-2 billion dollars in damages and more than 25 fatalities each year (USGS, 2009). The potential damage in Washington alone is estimated at tens to hundreds of billions of dollars (WA DNR, 2009). Washington has many potential triggers of landslides, including earthquakes, loss of rooting strength, rain on snow events, and human influence, but prolonged periods of high rainfall is the most commonly attributed trigger of landslides (WA DNR, 2009). Many hill slopes in the Olympic region of Washington State have failed recently due to increased rainfall infiltration and loss of suction.

Currently used slope stability analyses assume the pore water pressures above the phreatic surface to be equal to zero. Stability analysis procedures determine a factor of safety for the slope given the distribution of static positive pressures along the slip surface. In this method, the only way to evaluate the influence of climatic conditions, such as rainfall or ground surface flow, is to increase or decrease the phreatic surface, only looking at the static condition. Therefore, the influence of soil suction is generally ignored. Also, the estimation of soil properties such as internal friction angle and effective cohesion is done through back calculating known slope failures. If soil suction

was not included in the back calculation of the slope failure, the soil properties used for further analysis may be incorrect.

To correct the static phreatic surface analysis errors, a hydrology model that can be prescribed with varying vegetation and climate realizations should be used along with a stability model that includes soil suction. Similar studies have been conducted in other regions such as the tropics and Hong Kong, but there is a need to expand this approach to the Olympic region of Washington State as that region differs from others by having many shallow planar slope failures.

1.2 Objectives

The primary objectives of this study relate to the investigation of the effects of reduced soil suction on slope stability with increases in rainfall. The specific objectives of this study are as follows:

1. Develop a combined hydrology and slope stability model to model changes in pore water pressure due to rainfall infiltration, evaporation, and surface water retention. Use this information to determine its effect on shallow planar slope stability.

2. Validate the ability of the model to predict slope failures by comparing modeled failures to field case studies of previous slopes failures in the Olympic Region. Methods to identify model parameters will be developed.

3. Develop a chart for routine design applications using a range of slopes, vegetation conditions, and rainfall events.

1.3 Organization of Thesis

      This thesis is organized into 6 chapters. Chapter 2 is comprised of a literature review of the importance of soil suction and the need for coupling hydrologic information with slope stability analysis. It also introduces the basics of the Combined Hydrology and Stability Model (CHASM) program utilized in the study. The derivation of the infinite slope stability model, including soil suction, is presented in Chapter 3. Chapter 4 illustrates the validation of the model for use in the Olympic Region of Washington. Chapter 5 presents a design chart with appropriate changes in parameters that can be used for future design applications. The final chapter concludes all the major findings presented in this thesis.

CHAPTER 2

LITERATURE REVIEW

Shallow landslides, typically translational slope failures a few meters thick of unlithified soil mantle or regolith, may dominate mass-movement processes in hillslope environments (USGS, 2009). They are particularly destructive when they initiate or coalesce to form debris flows. Shallow landslides and debris flows are commonly triggered by intense precipitation or strong ground shaking and may affect extensive areas during a single meteorological or seismic event (USGS, 2009). Recent advances in the scientific understanding of landslide initiation, particularly for those landslides that occur under intense or prolonged precipitation in hillslope environments around the world, indicate that the failure surface may be above the water table and under nearly saturated conditions (Wray, 1984).

The classic methodology for landslide analysis assumes that earthen materials are either fully saturated or completely dry, neglecting the varying soil suction with varying moisture content contribution to the stability of slopes. Thus this methodology is overly conservative and incapable of accurately forecasting shallow land sliding. Recent advances in soil mechanics have shed light on the state of stress in partially saturated soil masses. Furthermore, physical evidence and scientific understanding in both geomechanics and geomorphology all point to the likelihood that the failure surface of infiltration-induced landslides may occur above the water table and under nearly saturated conditions (Wu and Likos, 2004).

It is evident that the shallow slide failures often as a result of infiltration from

rainfall. Therefore, analysis methods that combine hydrological information and slope

stability analysis are required. This literature review is thus focused on soil suction and

how suction has been utilized in slope stability analyses followed by a model that

combines hydrologic and slope stability into one program.

2.1 Soil Suction

Researchers had been looking at the relationship between soil-water-plant systems

when they first developed the theoretical concept of soil suction in the early 1900's

(Buckingham, 1907; Gardner and Widtsoe, 1921; Richards, 1928, Schofield, 1935;

Edlefsen and Anderson, 1943; Childs and Collis-George, 1948; Bolt and Miller, 1958;

Corey and Kemper, 1961; Corey et al., 1967). Since then, quantitative definitions of

soil suction have become accepted concepts in the geotechnical engineering field (Krahn,

and Fredlund, 1972; Wray, 1984; Fredlund and Rahardjo, 1988; Fredlund and Rahardjo,

1993).

Total suction consists of two main free energy components, matric and osmotic

suction; all other suction components such as gravitational and pressure suctions are

relatively small, therefore negligible (Fredlund and Rahardjo, 1993). According to the

review panel for the 1965 Soil Mechanics Symposium (Aitchison, 1965), matric suction

is suction derived from the partial pressure of the water vapor in equilibrium with the soil

water, in relation to the partial pressure of the water vapor in equilibrium with a solution

identical in composition with the soil water. Matric suction is commonly written as (u_a-

u_w) or the pore pressure of air minus the pore pressure of water. Osmotic suction is the

suction derived from the of partial pressures of the water vapor in equilibrium with a solution identical in composition with the soil water, relative to the partial pressure of water vapor in equilibrium with pure water, according to the 1965 Soil Mechanics Symposium review panel (Aitchison, 1965). Combining the two main free energy components of total suction can be written as

$$\Psi = (u_a - u_w) + \pi \qquad \text{(2-1)}$$

where *(u_a-u_w)* is matric suction and π is osmotic suction.

The main factors that affect matric suction are relative compaction, water content, and particle size. At low degrees of saturation with small particle size, pore-water pressure can be highly negative, even as low as 7MPa (Olson and Langfelder, 1965). The low pore water pressure results in very high matric and total suctions.

2.1.1 Krahn and Fredlund (1972)

Krahn and Fredlund (1972) conducted independent laboratory tests to determine the matric, osmotic, and total suction where dry densities and water content were used as the basis for comparison of all suction components. Matric suction was determined using a Modified Anteus Consolidometer developed at the University of Saskatchewan (Pufahl, 1970). The saturation extract technique electrical conductivity (USDA Agricultural Handbook No. 60, 1950) was used to determine the Osmotic suction. The psychrometer theory and operational technique utilizing relative humidity was utilized to determine total suction.

The measured soil suction values for Regina Clay and Glacial Till found in Saskatchewan, Canada compacted to AASHTO standards is given in Table 2-1 (Krahn

6

and Fredlund, 1972). The measured plastic limit and liquid limit are 31% and 78%,

respectively, for Regina Clay and 17% and 34% for the Glacial Till. As one can see, the

total suction values under optimum suction conditions are quite high and have potential

to significantly affect the soil strength.

Soil Type	Water Content (%)	Matric Suction, (uw-ua) (kPa)	Osmotic Suction, π (kPa)	Total Suction, ψ (kPa)
Regina Clay: γ_{max} = 13.81 kN/m^3	30.6 (optimum) 28.6	273 354	187 202	460 556
Glacial Till: γ_{max} = 19.24 kN/m^3	15.6 (optimum) 13.6	310 556	290 293	600 849

Table 2-1: Typical suction values for different soils (Krahn, and Fredlund, 1972)

2.1.2 Lim et al. (1996)

In 1996, Lim et al. conducted a field instrumentation program that continuously

and simultaneously measured the in-situ matric soil suction and rainfall on a residual soil

slope in Singapore. The slope was divided into three sections with differing surface

conditions (canvas over grass, grass, and bare soil). Figure 2-1 presents the measured

soil suction values before and after a rainfall recorded on February 6, 1994 in which R1,

R2, etc. are different location along the slope.
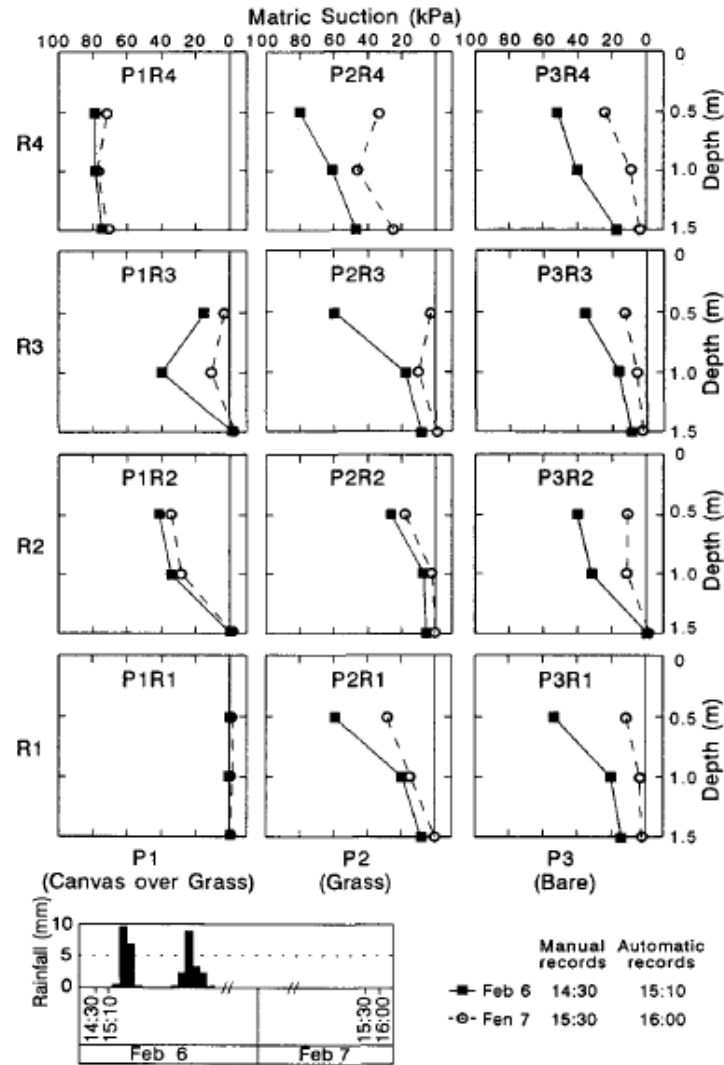
Figure 2-1: Lim et al. (1996) Changes in in-situ soil suction conditions due to rainstorm

event of February 6, 1994

Lim et al. (1996) concluded that the variation of matric suction is less significant under the canvas covered slope than for the other two sections. However, presence of vegetation on the slope significantly increased the soil suction on the slope and altered the total head profile within the slope. The study and field observations are useful in displaying the importance of surface conditions and flux boundary conditions when modeling soil suction on a slope.

2.2 Stability Models Including Soil Suction

While not commonly utilized in practice, stability models that include soil suction have been developed and validated in the field.

2.2.1 Griffiths and Lu (2005)

Griffiths and Lu (1995) presented a framework for slope stability analysis that estimated the effect of soil suction on the stability of slopes by changing the effective stress of the soil as developed by Lu and Likos (2004) rather than altering the shear strength of the soil as presented by Fredlund et al. (1978). This study utilized Equation 2-2 presented by Lu and Likos (2004) that unifies saturated and unsaturated conditions, to estimate the effects of soil suction on the effective stress of the soil.

$$\sigma' = (\sigma - u_a) - \sigma^s \qquad \text{(2-2)}$$

In Equation 2-2, u_a is the pore air pressure and σ^S is the suction stress as determined by the suction stress characteristic curve (Lu and Likos, 2004). Once the effective stress was determined that included soil suction, an elasto-plastic finite element analysis was used to evaluate the stability of slopes under steady seepage conditions (Griffiths and Lu, 2005).

Finite element stability analyses were conducted on two homogeneous slopes, one silt and the other clay to evaluate the effects of seepage and evaporation on slope stability (Griffiths and Lu, 2005). Figures 2-2 and 2-3 show the effect of seepage and evaporation on the silt and clay profile as determined by the finite element analysis.
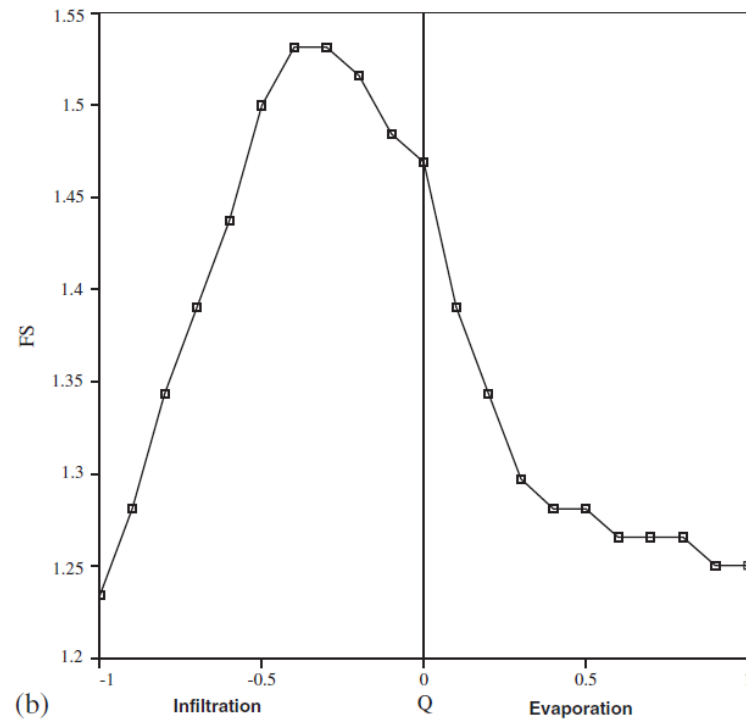
Figure 2-2: Griffiths and Lu (2005) Influence of infiltration and evaporation on the factor

of safety for a silt slope
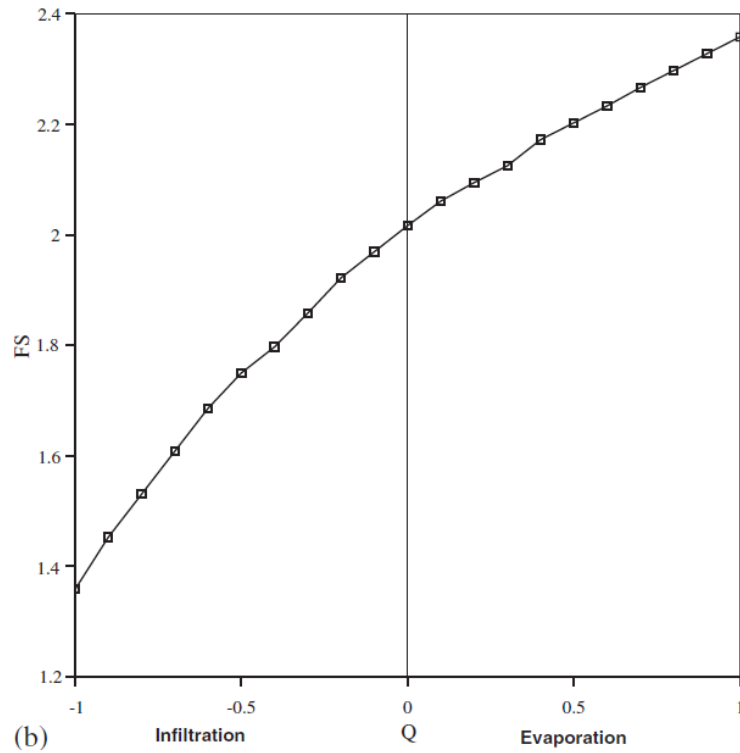
Figure 2-3: Griffiths and Lu (2005) Influence of infiltration and evaporation on the factor

of safety for a clay slope

The study determined that for a clay slope, evaporation increases the slope factor

of safety while infiltration decreases it (Griffiths and Lu, 2005). For the silt slope,

however, both high infiltration and high evaporation decrease the slope stability with the

maximum stability reached for intermediate values, because the influence of soil suction

is reduced in the larger soil matrix of silt under dryer conditions.

The study further showed how soil suction can affect the stability of both silt and

clay slopes. However, because the studied slopes were homogeneous and the

infiltration/evaporation rates were held constant, the study has limited usage for real

world slope conditions. Also, in order to estimate the effects of soil suction on the slope

a suction stress characteristic curve was estimated, which requires extensive shear

strength testing of soils under various moisture conditions or theoretical formulations.

The finite element stability analysis procedure does have practical applications with more complex soil profiles and for accurate predictions of soil suction, however.

2.2.2 Lu and Godt (2008)

Lu and Godt (2008) conducted a very similar study to Griffiths and Lu (2005) in that the suction effects on slope stability were considered using the suction effect on effective stress rather than shear strength. However, traditional infinite slope stability equations were then used to determine the stability of slopes using the altered effective stress parameter, rather than elasto-plastic finite element analysis. The infinite slope stability method is widely used in practice for its simplistic approach to stability analysis while remaining accurate for many slope conditions.

The study validated their framework by performing a theoretical parametric study on a variety of sandy and silty soils using steady seepage rates in the estimation of the soil suction parameter (Lu and Godt, 2008). A case study was also conducted by Lu and Godt (2008) on a highly instrumented costal bluff along the Puget Sound in which they were able to show failure of the slope when the maximum daily infiltration was applied to the slope. Figure 2-4 shows the estimation of factors of safety in relation to the distance above the water table for 0 infiltration, the monthly maximum infiltration, and the daily maximum infiltration.
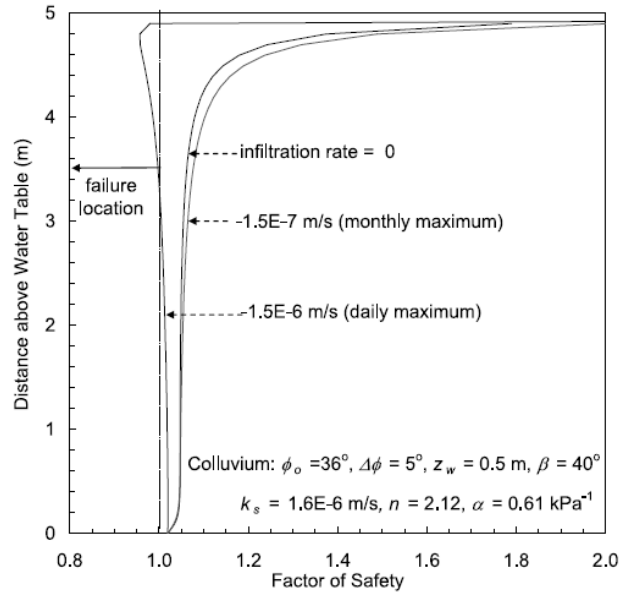
Figure 2-4: Lu and Godt (2008) Variation of factor of safety with depth for the case study of costal bluffs along the Puget Sound

While Lu and Godt (2008) were able to effectively estimate the soil suction parameter in slope stability and properly estimate slope failure in the case study, the study only looked at the steady seepage condition which rarely occurs in nature. The suction stress characteristic curve determination requires extensive shear strength testing of soils under various moisture conditions (Lu and Likos; 2004, 2006). The shear strength testing would make very accurate predictions of suction effects for specific slopes, but would become impractical for generalized slopes over a large region.

2.3 Combined Hydrology/Stability Model (CHASM)

Anderson and Lloyd (1991) developed CHASM to incorporate vegetative and soil suction effects on slope stability. CHASM initially utilized a two-dimensional finite difference hillslope hydrology model to predict the transient pore water pressures. The

13

hydrology model structure is presented in diagram format in Figure 2-5. The model

outputs pore water pressures for each specified time step throughout duration of the

model.
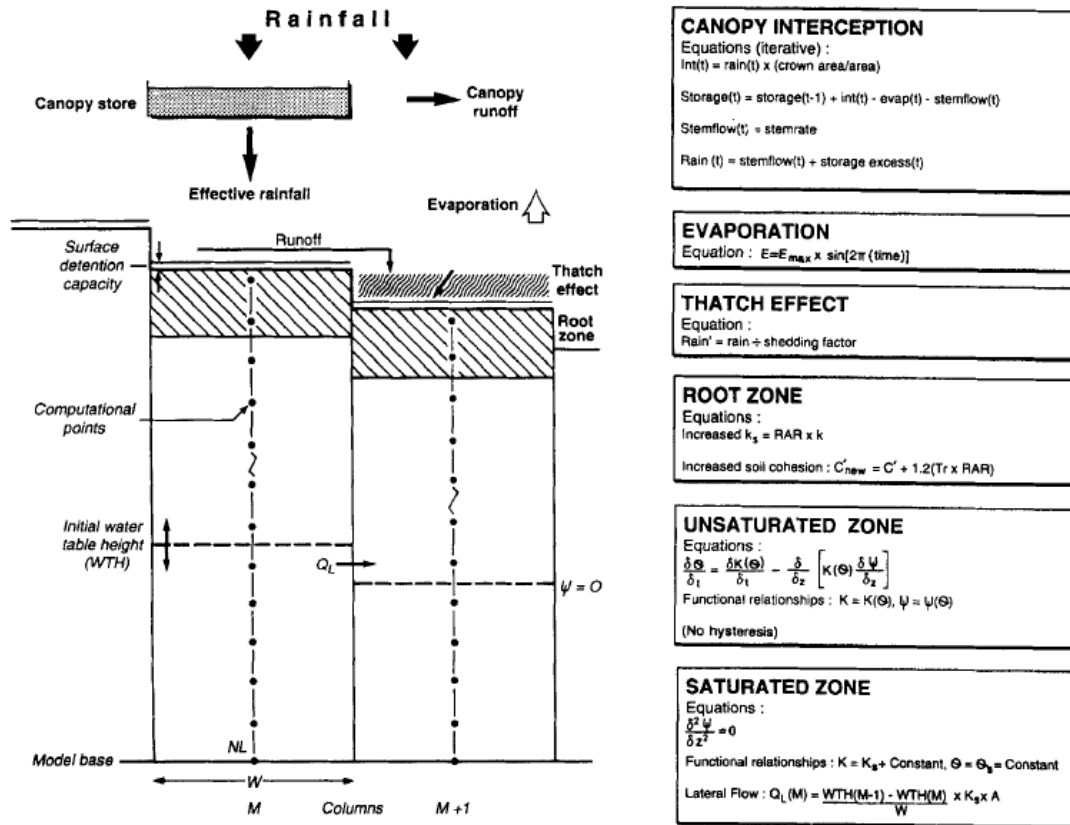
Figure 2-5: Collison and Anderson (1996) CHASM hydrology model structure

Pore pressure data (positive or negative) were then incorporated into the two-

dimensional slope stability model. The stability model searches various failure surfaces

for the lowest factor of safety for a given time step to determine slope safety.

2.3.1 Wilkinson et al. (2002)

Wilkinson et al. (2002) extended CHASM's modeling capabilities by

incorporating hydrological controls such as hillslope soil-water convergence and

vegetation cover that have direct impacts on pore water pressures into a three-

dimensional model. CHASM's hydrology model is a forward explicit finite difference

scheme. Figure 2-6 shows the general schematic of the three-dimensional hydrology

model. The model has the capability of simulating detention storage, infiltration,

evaporation, and unsaturated and saturated flow. Rainfall is allowed to infiltrate at the

top of the cells after any rainfall interception and evaporation rates have been deducted at

a rate governed by the infiltration capacity. Unsaturated flow is only assumed to take

place in the vertical direction per Marshall and Holmes (1979). Saturated flow between

columns is modeled using Darcy's (1856) equation for saturated flow.
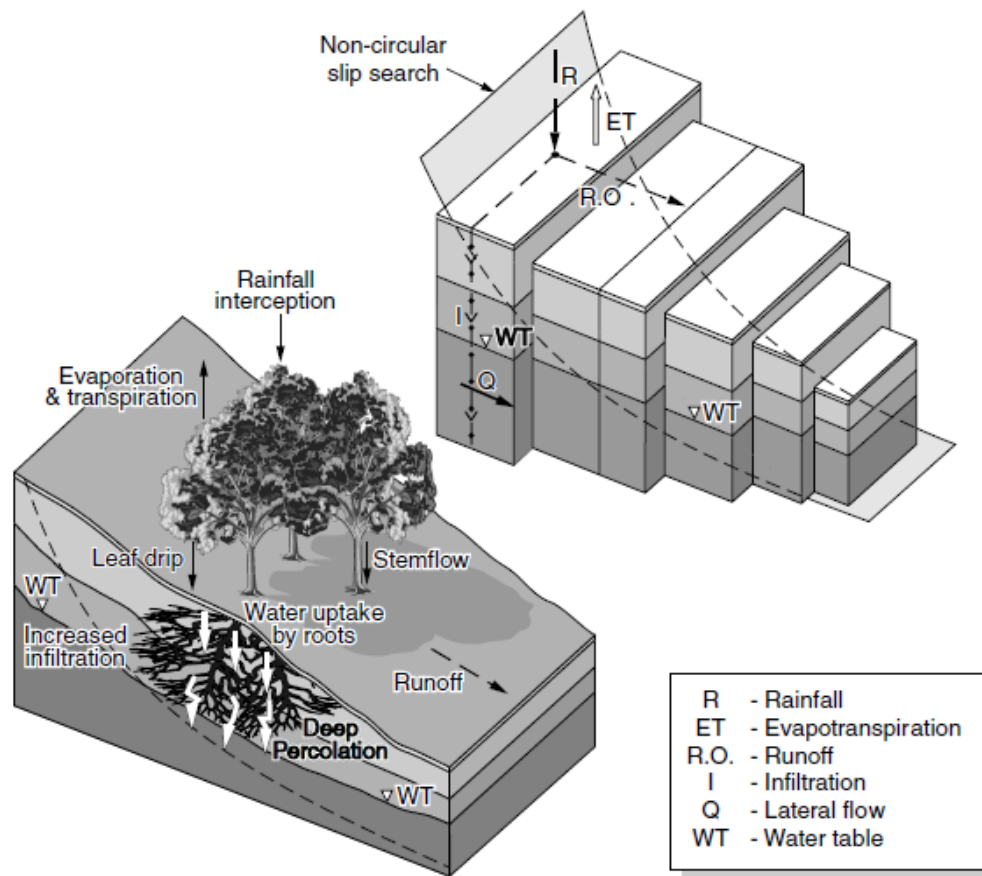
Figure 2-6: Wilkinson et al. (2002) Hydrology model structure

At each time step of the simulation, the hydrology model results are directly input into a limit equilibrium model for slope stability. Pore pressures, positive and negative, are incorporated directly into the effective stress determination of the Mohr-Coulomb equation for soil shear strength.

The following are the hydrology mechanism equations that make up the hydrology model:

Rainfall interception for grasses is simply modeled as a reduction in hourly rainfall intensity applied to the surface of the slope. For trees, the more complex interception model is described by the free throughfall coefficient, stemflow-partitioning coefficient, canopy storage capacity, and trunk storage capacity (Rutter et al., 1971; Valente et al., 1997). The dynamic calculation of the water balance equations for tree infiltration is described as follows in Equations 2-3 and 2-4:

$$(1 - p - p_t)\int R dt = \int D dt + \int E dt + \Delta C \qquad (2\text{-}3)$$

$$p_t \int R dt = S_f + \int E_t dt + \Delta C_t \qquad (2\text{-}4)$$

R is the intensity of the gross rainfall, D is the rate of drainage from the canopy, E is the evaporation rate of the water intercepted by the canopy, ΔC is the change in canopy storage, S_f is the stemflow, E_t is the evaporation rate of the water intercepted by the trunks, and ΔC_t is the change in the trunk storage.

Evapotranspiration and root water uptake reduce the amount of water within the soil. Potential evapotranspiration is determined using the Penman-Monteith equation, Equation 2-5.

$$E_p = \frac{\Delta R_n + \rho c_p VPD / r_a}{\lambda [\Delta + \gamma (1 + r_c / r_a)]} \qquad (2\text{-}5)$$

E_p is the potential evapotranspiration rate, r_a and r_c are aerodynamic and canopy

resistances respectively, Δ is the slope of the saturation vapor pressure-temperature curve,

VPD is the vapor pressure deficit, c_p is the specific heat of the air, and R_n is the net

radiation term. Under saturated conditions, the leaf stomata close. Therefore, canopy

resistance (r_c) was set to zero (Wilkinson et al., 1998). To link the actual transpiration

rates to actual root water uptake, the hourly transpiration values were converted to meters

per second using Equation 2-6.

$$T_v = \left(\frac{T}{\rho_w}\right)LAI \tag{2-6}$$

T is the transpiration flux density, T_v is the transpiration rate, ρ_w is the density of water,

and LAI is the leaf-area index. To calculate the amount of moisture removed from the

soil, transpiration extraction was varied with depth according to root density with the

maximum rate of water uptake determined by Equation 2-7 from Feddes et al. (1976).

$$S_{max} = T_v / z_r \tag{2-7}$$

S_{max} is the maximum root uptake and z_r is the root depth. If the soil is either too dry or

too wet, the maximum root uptake is reduced by Equation 2-8.

$$S(h) = \alpha(h)S_{max} \tag{2-8}$$

S(h) is the actual root water uptake and $\alpha(h)$ is a dimensionless factor based on the

pressure head. For each time step, the water uptake for each cell containing roots acts as

an uptake in Equation 2-5. Therefore, the final hydraulic effect is concerned with the

increase in hydraulic conductivity as a result of the root network. The magnitude of this

effect is determined by Equation 2-9 (Collison, 1993; Collison et al 1995) relating root-

area to the saturated hydraulic conductivity.

$$\Delta K_s = \alpha + \beta RAR \qquad \qquad (2\text{-}9)$$

ΔK_s is the increase in saturated hydraulic conductivity, α and β are constants and RAR is the root-area ratio.

Wilkinson et al. continued to model the effect of vegetation on slopes by taking into consideration the apparent increase in cohesion due to root strength and the additional surcharge due to vegetation. These effects were taken into consideration in Bishop's limit equilibrium equations to determine the factor of safety for each time step in the analysis. The study was validated by a case study of the Hawke's Bay region of New Zealand.

The hydrology modeling capabilities of CHASM presented by Wilkinson et al. accurately predict the soil pore water pressure allowing for the estimation of soil suction within a hillslope profile. However, since CHASM uses Bishop's failure surface, which is a deep seated failure, the complete CHASM model is not representative of the shallow slope failures that occur in the Olympic region of Washington State. A combined hydrology/stability model that incorporates the hydrology model of CHASM with the shallow landslide failure mechanism is needed to accurately determine the stability of slopes in the Olympic region of Washington State.

CHAPTER 3

INFINITE SLOPE STABILITY

3.1 Failure Mechanisms

Slope failures that occur parallel to the surface of the slope and extend a relatively

long distance to the depth of the failure may be analyzed as an infinite slope failure,

where the influence of the end effects of the failure are ignored (Sharma, 1996). Shallow

failures are often triggered by increased water in the upper soil layer caused by heavy

precipitation or snowmelt (Wieczorek, 1996). The geological conditions that typically

lead to slope failures that can be analyzed as infinite are very shallow failures composed

mostly of soil located above the rooting depth of trees. Other failures that can be

analyzed as an infinite slope failure are cohesionless soils, colluvial soils over shallow

rock, or stiff fissured clays within the upper highly weathered zone (Sharma, 1996). In

cases for which the failure is categorized as an infinite slope failure, limit equilibrium

methods can be applied to their analysis.

3.2 Dry Cohesionless Soil

The simplest form of the infinite slope equation is used for dry cohesionless soils

in which the free body diagram used to determine driving forces and resisting forces can

be seen in Figure 3-1.
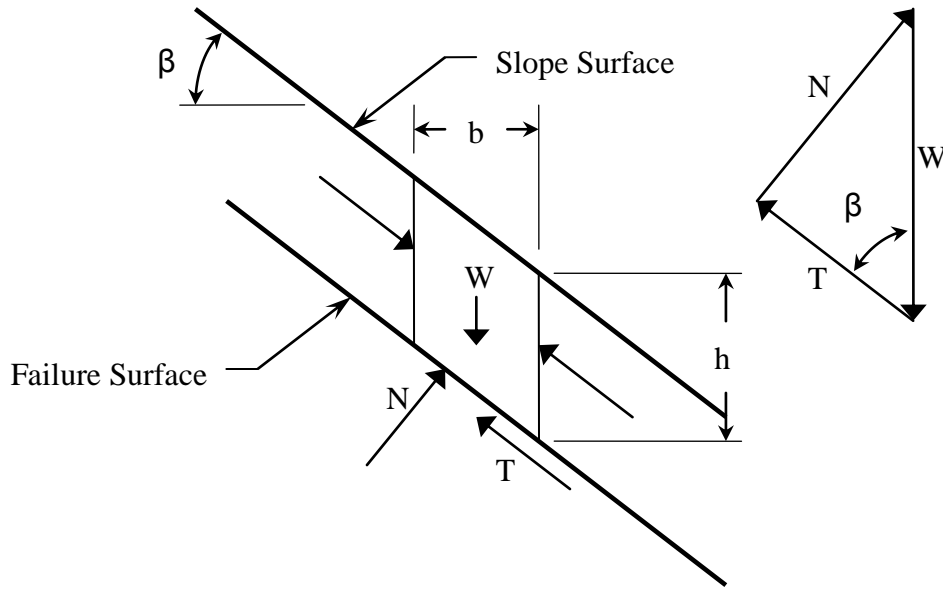
Figure 3-1: Free body diagram of infinite slope analysis for dry cohesionless soil

The weight of each slice, *W*, can be determined by *γ,* soil unit weight, *b,* width of the slice, and *h,* height of the slice as:

$$W = \gamma bh(1) \tag{3-1}$$

Here, 1 is the unit dimension into the page to give the slope a third dimension. The normal forces, *N*, and driving forces, *T*, then can be determined as:

$$N = W\cos(\beta) \tag{3-2}$$

and

$$T = W\sin(\beta). \tag{3-3}$$

where *β* is the angle of the slope. For Mohr-Coulomb type failure, the resistance force, *S,* along the slope failure is dependent upon the internal friction angle, *Φ,* of the soil and can be written as:

$$S = N\tan(\phi) \tag{3-4}$$

Using the limit equilibrium principle, the Factor of Safety, *FOS*, can then be written as

$$FOS = \frac{N\tan(\phi)}{W\sin(\beta)} \qquad\qquad (3\text{-}5)$$

or

$$FOS = \frac{\tan(\phi)}{\sin(\beta)} \qquad\qquad (3\text{-}6)$$

for a simple dry cohesionless slope.

By examining this solution, one can see that the slope height and slope have no effect on stability. Also, in order to have a stable slope *FOS* greater than one the slope angle, β, must be smaller than the angle of internal friction, Φ, or angle of repose.

3.3 Saturated Soil with Cohesion

The same limit equilibrium concepts could now be applied for saturated soils with cohesion and the seepage line at the surface of the slope, but now the *FOS* is more complex and must include effective forces. The resisting force acting along the failure plane, *S*, now depends on effective cohesion of the soil, c_s', and effective internal friction angle, Φ', and can be written as

$$S = c_s' b\sec(\beta) + (N - U)\tan(\phi'). \qquad\qquad (3\text{-}7)$$

The pore water pressure acting at the base of the failure, *U*, can be written as

$$U = \frac{\left[\gamma_w h\cos^2(\beta)\right]b}{\cos(\beta)} \qquad\qquad (3\text{-}8)$$

or

$$U = \gamma_w bh\cos(\beta). \qquad\qquad (3\text{-}9)$$

21

where γ_w is the unit weight of water. The *FOS* for saturated soil with cohesion can then be written as

$$FOS = \frac{c'_s b \sec(\beta) + (N - U)\tan(\phi')}{W \sin(\beta)}.$$
(3-10)
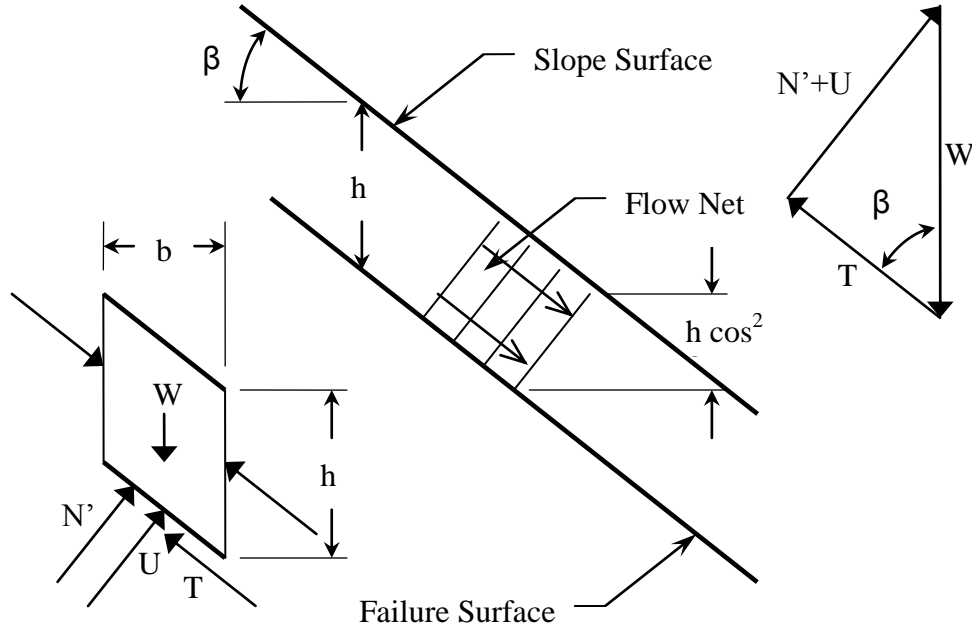
Figure 3-2: Free body diagram of infinite slope analysis for saturated soil with cohesion

The weight of each slice term for saturated soil is:

$$W = \gamma_{sat} bh$$
(3-11)

substituting Eq. (3-11) into (3-10) and rearranging we get:

$$FOS = \frac{c'_s + h\cos^2(\beta)(\gamma_{sat} - y_w)\tan\phi'}{\gamma_{sat} h \sin(\beta)\cos(\beta)}.$$
(3-12)

3.4 Moist Soil with Cohesion

Extending the analysis when the seepage line is assumed to be a depth mz above the failure surface, the FOS is given by (Sivakugan and Das, 2010)

$$FOS = \frac{c_s' + h\cos^2(\beta)\left[(1-m)\gamma_m + m\gamma'\right]\tan\phi'}{h\sin(\beta)\cos(\beta)\left[(1-m)\gamma_m + m\gamma_{sat}\right]} \tag{3-13}$$
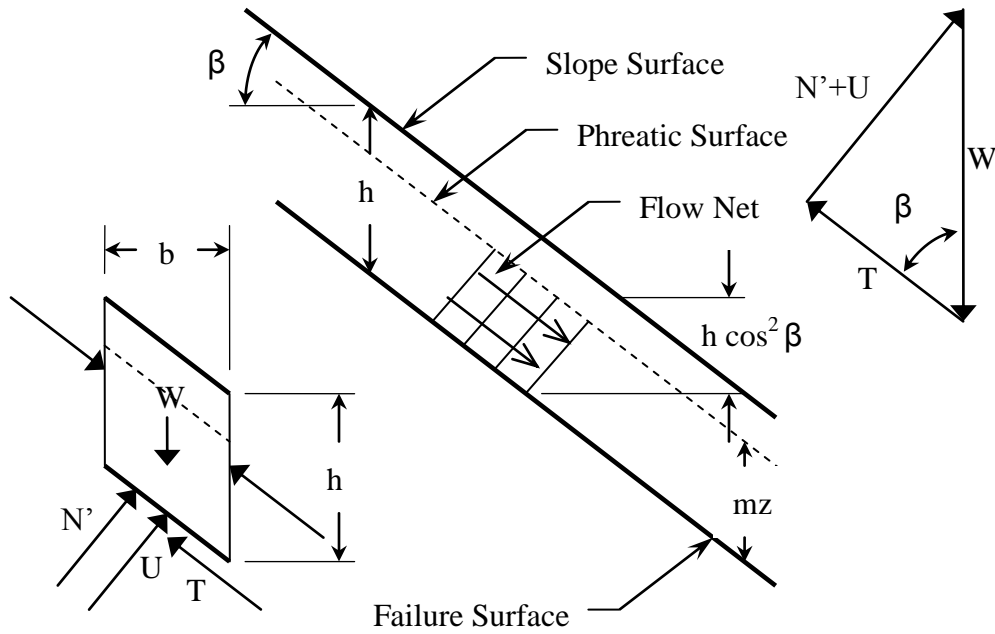
Figure 3-3: Free body diagram of infinite slope analysis for moist soil with cohesion where the fraction m lies between 0 and 1.

$$\gamma' = \gamma_{sat} - \gamma_w \tag{3-14}$$

γ_{sat} and γ_m are saturated and moist soil unit weights below and above the seepage line, respectively. Substituting y', Equation 3-13 is expanded as:

$$FOS = \frac{c_s' + h\cos^2(\beta)\left[(1-m)\gamma_m + m(\gamma_{sat} - \gamma_w)\right]\tan\phi'}{h\sin(\beta)\cos(\beta)\left[(1-m)\gamma_m + m\gamma_{sat}\right]} \tag{3-15}$$

By introducing variables D_m, D_w, and D for depth of moist soil [*(1-m)h*], depth of saturated soil [*mh*], and depth of failure [*D*], respectively, the following equation may be established, in which one can find the critical depth of a failure surface for any seepage condition by setting the FOS to 1.

$$FOS = \frac{c'_s + \cos^2(\beta)[D_m\gamma_m + D_w(\gamma_{sat} - \gamma_w)]\tan\phi'}{\sin(\beta)\cos(\beta)[D_m\gamma_m + D_w\gamma_{sat}]} \qquad (3\text{-}16)$$

3.5 Vegetation

Vegetation on a slope can affect the stability of the slope in many different ways, both positively and negatively, through the following mechanisms: interception, evapotranspiration, root water up take, leaf drip, stem flow, hydrologic conductivity, root reinforcement, and surcharge (Wilkinson et al. 2002). In this infinite slope stability model, the will focus is on the mechanical effects of reinforcing of the soil by vegetation roots and the increase in surcharge due to the weight of the large firs and spruce-hemlock generally covering the Olympic Region of Washington.

3.6 Roots

The simplest mechanical model to consider the increase in soil strength due to root reinforcement assumes an isotropic reinforcement. Because no root system is completely isotropic and root morphology can vary greatly, a true solution to root reinforcement would be too complex to model properly. However, it is possible to outline the general concepts of root reinforcement using the isotropic model. The increase in stress can be given by Wu (1984)

$$\sigma_R = T_R \left(\frac{A_R}{A} \right) \tag{3-17}$$

in which T_R, A_R, and A are the tensile stress in the root reinforcement at the time of failure, the cross sectional area of the root along the slip plane, and the total area of the slip plane, respectively (Wu 1984). The strength increase due to reinforcement can be characterized by an increase in soil cohesion, c'_R (Hausmann 1978),

$$c'_R = \frac{\sigma_R}{2\sqrt{K_a}} \tag{3-19}$$

where $K_a = \tan^2\left(45 - \frac{\phi}{2}\right)$ is the active earth pressure coefficient. Incorporating the increase in root strength into the previously established infinite slope stability equation results in:

$$FOS = \frac{c'_s + c'_R + \cos^2(\beta)\left[D_m\gamma_m + D_w(\gamma_{sat} - \gamma_w)\right]\tan\phi'}{\sin(\beta)\cos(\beta)\left[D_m\gamma_m + D_w\gamma_{sat}\right]} \tag{3-20}$$

3.6.1 Soil root interaction model

For situation in which the potential slope failure intersects the roots of a tree, shown in Figure 3.4, the roots must fail in tension, shear, or bond or some combination of the three (Wu 1984). To evaluate the contributions of the roots on the soil, the shear forces R_s, normal forces R_n, and moment forces R_M the roots can withstand must be determined. If the roots are small and flexible, they are not able to withstand moment forces; therefore, the moment can be assumed to be zero (Wu 1983.) Often the shear strength of the roots is much larger than the shear strength of the soil, causing flexible roots to deform along the slip surface rather than shear. Another assumption that can be

made to simplify the model is that θ is 90° (Wu 1984). Only a combination of bond and tension failure remains to resist slope failure. Laboratory test by Burroughs and Thomas (1976), Gray (1978), and Turmanina (1965) have all contributed to the estimation of the average tensile strength of different tree species which can be used in Equation 3-17.
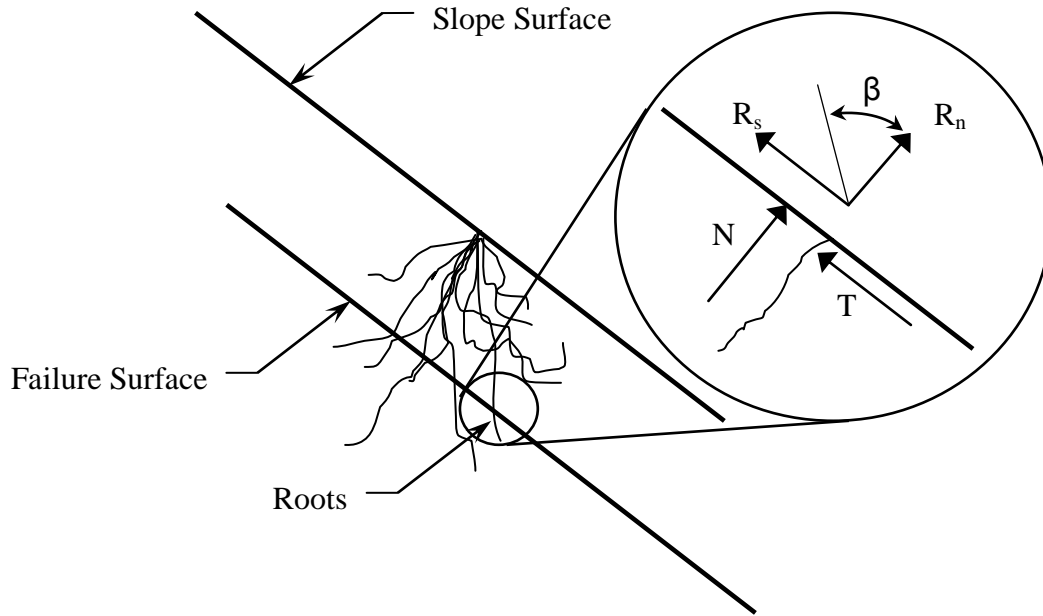
Figure 3-4: Root Forces at the failure plane

3.7 Surcharge

The total weight of soil above the potential failure plane typically far exceeds the weight of vegetation (O'Loughlin and Ziemer, 1982). Therefore, the surcharge from additional weight of vegetation on the soil is normally considered for trees only since the weight of most grasses and shrubs is nominal. In this model, the surcharge is assumed to be distributed uniformly over the entire hill slope. Surcharge increases the down slope forces on the slope, resulting in an increase in the driving force of the soil.

$$S_w \sin(\beta)\cos(\beta) \tag{3-21}$$

Surcharge also increases the frictional resistance of the soil along the failure surface.

$$S_w \cos^2(\beta)\tan(\phi') \qquad (3\text{-}22)$$
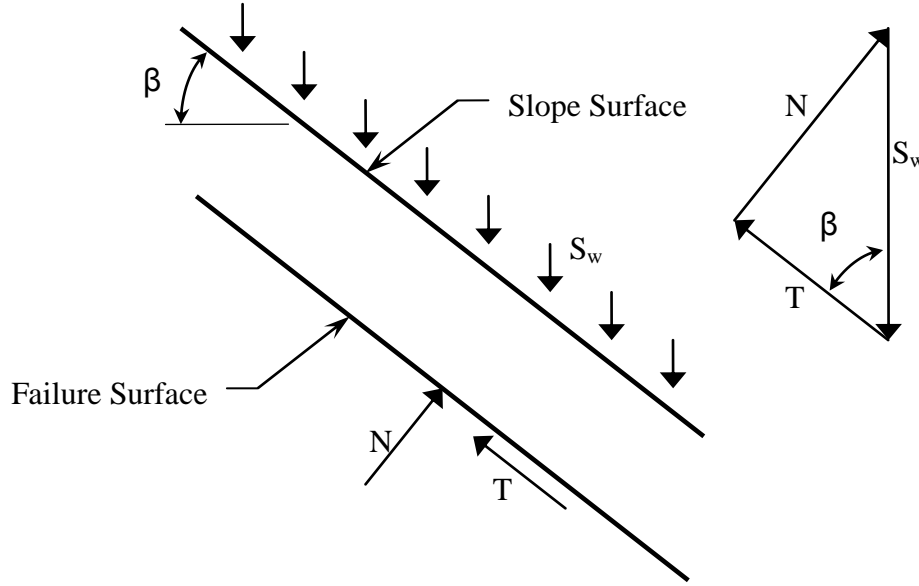
Figure 3-5: Free body diagram of infinite slope analysis with surcharge

By combining the two effects of surcharge, a change in the FOS can be shown to be due to the surcharge from densely forested slopes, as follows:

$$\Delta FOS = \frac{S_w \cos^2(\beta)\tan(\phi')}{S_w \sin(\beta)\cos(\beta)} \qquad (3\text{-}23)$$

Accounting for the effect of surcharge in Eq. (3-18), the FOS becomes:

$$FOS = \frac{c_s' + c_R' + \cos^2(\beta)\left[D_m \gamma_m + D_w(\gamma_{sat} - \gamma_w) + S_w\right]\tan\phi'}{\sin(\beta)\cos(\beta)\left[D_m \gamma_m + D_w \gamma_{sat} + S_w\right]} \qquad (3\text{-}24)$$

Coastal forest types of the Pacific Northwest have surcharges ranging from 1 to 5 *kPa* for mature forests (Bishop and Stevens (1964), O'Lloughlin (1974), Wu et al. (1979)). More accurate estimations of surcharge can be calculated from timber inventory data if detailed information on tree size and distribution is available for the location to be

analyzed. However, this level of analysis is rarely necessary due to the small effect

vegetation surcharge has on the slope.

3.8 Soil Suction

To incorporate the influence of matric suction on the shear strength of the soil in

the vadose zone, Fredlund et al (1978) proposed that soil suction be viewed as an increase

in soil cohesion. Accordingly, matric suction can be written as:

$$c^b = (u_a - u_w)\tan\phi^b \qquad (3\text{-}25)$$

where $(u_a\text{-}u_w)$ and Φ^b are the pore pressure of the air minus the pore pressure of water and

friction angle with respect to matric suction, respectively. Thus, the effect of soil suction

on the factor of safety is as follows:

$$FOS = \frac{c^b}{1} = \frac{(u_a - u_w)\tan\phi^b}{1} \qquad (3\text{-}26)$$

Incorporating this into the previous model we get:

$$FOS = \frac{c_s' + c_R' + \cos^2(\beta)[D_m\gamma_m + D_w(\gamma_{sat} - \gamma_w) + S_w]\tan\phi' + (u_a - u_w)\tan\phi^b}{\sin(\beta)\cos(\beta)[D_m\gamma_m + D_w\gamma_{sat} + S_w]} \qquad (3\text{-}27)$$

3.9 Hydrologic Model Incorporation

Many practicing engineers and geologists assume a water condition for slope

analysis based on prior knowledge and, if available, data from piezometers on the slope.

For this analysis, however, it is important to properly predict the actual water conditions

so that changes in vegetative cover can be taken into consideration. Also, an advanced

hydrologic model such as CHASM, as discussed in Section 2.3, allows for the prediction

28

of moisture content of soils above the phreatic surface which is important in predicting the effect of soil suction on the slope.

The finite difference scheme hydrologic model used in CHASM simulates detention storage, infiltration, evapotranspiration, and unsaturated and saturated flow. The model output is a matrix of cells along the slope at the given cell interval for each time period, iteration is on pore pressure and moisture content for each cell (Wilkenson et al., 2002).

To incorporate the output from the hydrologic model, the term D_c, depth of cells, which correlates to the size of the soil cells in the hydrologic model, must be introduced. Since the cell pattern is consistent throughout the slope, D_c will not change with depth of the soil, making it critical to select the correct cell depth when establishing the hydrologic model. The hydrologic model accurately predicts soil moisture and rarely predicts a dry soil condition (see Section 3.4) (Wilkenson et al., 2002). The soil unit weight above the failure surface is determined by summing the weight of the cells above the failure surface, $(\Sigma\gamma_m D_c)$. Each cell weight is determined from the soil unit weight and moisture content of that cell. Thus, in order to incorporate the CHASM hydrologic model output, the term $(\Sigma\gamma_m D_c)$ is substituted for the soil weight terms, $D_m\gamma_m + D_w\gamma_{sat}$, Where

$$\gamma_m = \gamma_d(1+w) \text{ (Holtz and Kovacs, 1981)} \qquad (3\text{-}28)$$

$$FOS = \frac{c_s' + c_R' + \cos^2(\beta)[(D_m + D_w(\gamma_{sat} - \gamma_w) + S_w]\tan\phi' + (u_a - u_w)\tan\phi^b}{\sin(\beta)\cos(\beta)[(\Sigma\gamma_m D_c) + S_w]} \qquad (3\text{-}29)$$

For the purposes of this study, it is assumed that the failure surface is above the phreatic surface, resulting in a failure due to reduction in soil suction. Therefore, the term $(\Sigma\gamma_m D_c)$ also can be substituted for $D_m\gamma_m + D_w(\gamma_{sat} - \gamma_w)$, resulting in:

$$FOS = \frac{c'_s + c'_R + \cos^2(\beta)\left[\left(\sum \gamma_m D_c\right) + S_w\right]\tan \phi' + \left(u_a - u_w\right)\tan \phi^b}{\sin(\beta)\cos(\beta)\left[\left(\sum \gamma_m D_c\right) + S_w\right]} \tag{3-30}$$

CHAPTER 4

MODEL VALIDATION

4.1 Selection of Validation Slopes

The Olympic Region of Washington State has very diverse geological, hydrological, and vegetative settings in which landslides occur. Two regions were chosen to define appropriate soil parameters and validate the developed combined hydrology-slope stability model. The validated model was subsequently used to develop the design charts shown in Chapter 5. The slopes, Queets River slope and Clallam River slope, were chosen to represent two differing geologic and geographical settings having similarity in shallow failure landslide type. Detailed information on the landslides and geologic profiles on these sites are found in the technical reports authored by Slaughter and his colleagues among others (Slaughter and Lingley Jr., 2006).

4.2 Queets River Slope

The Queets river landslide site was chosen for having had multiple shallow landslides occurring in the same vicinity within the same year. The site is located just north of the Queets River and Olympic National Park and is 16 kilometers (10 miles) east of the Washington coast (Figures 4-1, 4-2, and 4-3). The site slopes down to the west at a slope of approximately 1.28 : 1 into McKinnon Creek, a tributary of the Queets River. McKinnon creek presumably flowed water at the toe of the slope during the slope failures. Currently the site has not been developed with the exception of a logging road

that was installed near the crest of the slope to harvest the timber on the slope. The

landslides occurred downslope of an existing logging road.
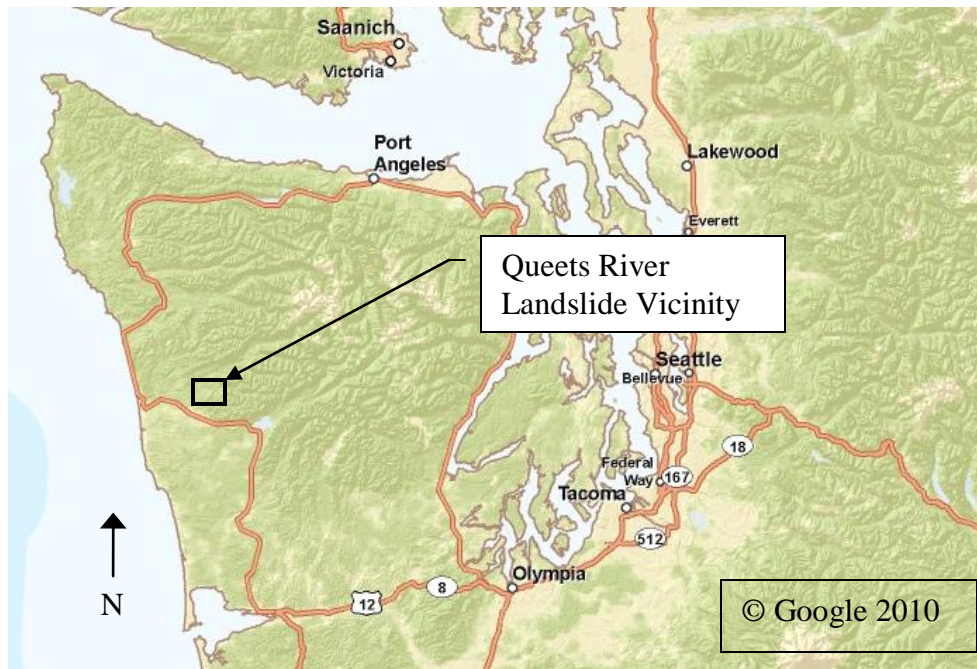
Figure 4-1: Vicinity map of Queets River Landslide
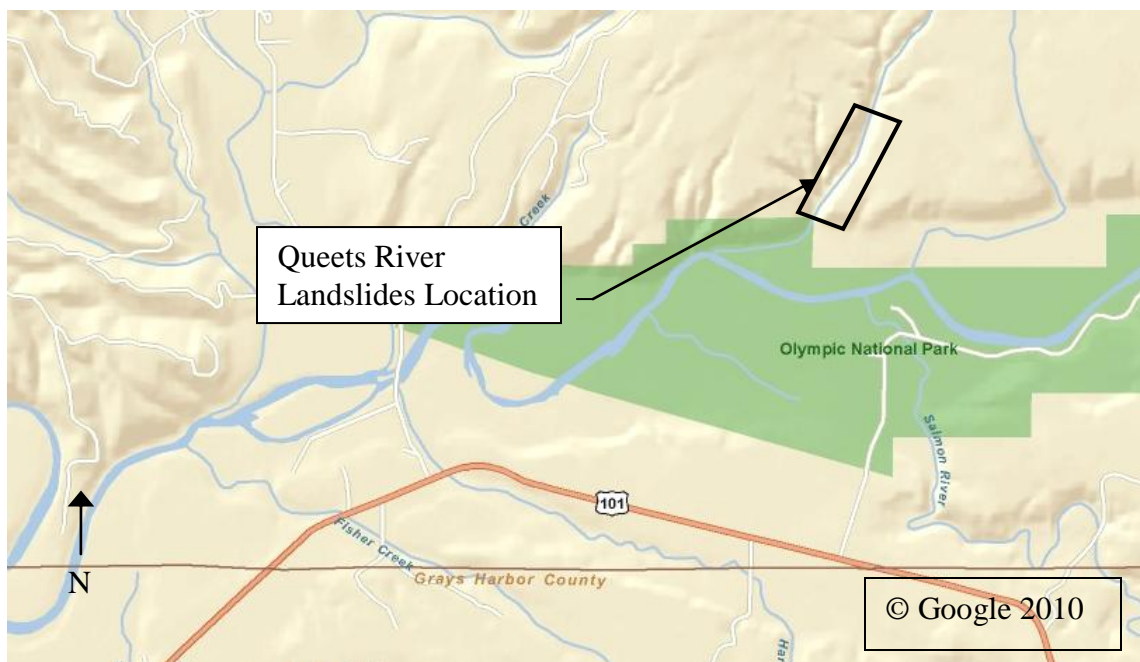
Figure 4-2: Site map of Queets River Landslide
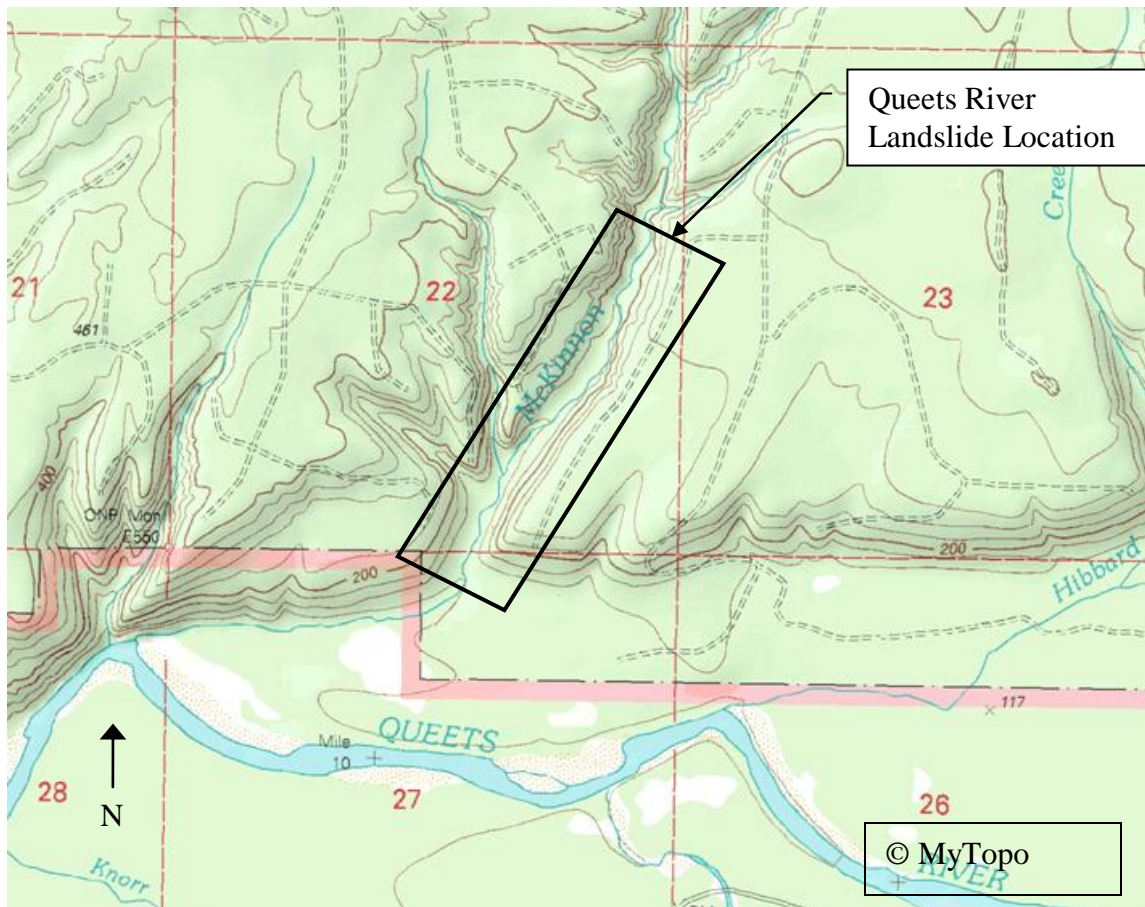
Figure 4-3: Topographical map of Queets River Landslide

4.2.1 Landslides

The information on the landslides at this site was gathered from the technical report by Slaughter and Lingley Jr. (2006). The four landslides at this site were first identified in 1985 and were classified as shallow rapid landslides that derived from heavy precipitation events. The landslides were between 120 and 370 square meters (0.03-0.09 acres) in size and occurred on gradients ranging from 60 to 69%. The landform was sensitive to any forest practice activity that reduces root strength, or otherwise disturbs the ground (Slaughter and Lingley Jr., 2006).

4.2.2 Slope description

The four landslides studied at this site occurred along the southeast slope of McKinnon creek basin. The site sloped down at a fairly constant rate of 1.28 : 1 for nearly all of the slides. The elevation difference between the crest of the failure and the toe of the failure of the slides were between 30 and 45 meters (100-150 feet) with a horizontal length of 55 to 95 meters (180-300 feet). Topographical maps of the region indicate that the slope studied appears to be representative of other slopes in the area.

4.2.3 Local geology

Geologic conditions are based on a review of geologic maps (Gerstel and Lingley, 2000 and Dragovich et al., 2002). Thin (3-10m) Alpine Glacial Outwash (Qapo) underlies the site. This soil was deposited during the early to mid-Wisconsinan age of the pre-Fraser Glaciation approximately 30,000 to 1.8 million years ago. The unit is described as stratified sand, gravel, and cobbles with local inclusions of peat, silt, clay and weathered loess; gray to subtle yellow weathering. Deposits are similar to the Late Wisconsinan alpine outwash (Qao) in grain size distribution, clast lithology, and bedding characteristics, but are weathered to 1-2m deep and are commonly capped by mottled tan-gray to pale orange silt and clayey silt (Loess). The Alpine Glacial Outwash deposits are generally weakly consolidated and consist of cobbles and gravel in a sand matrix.
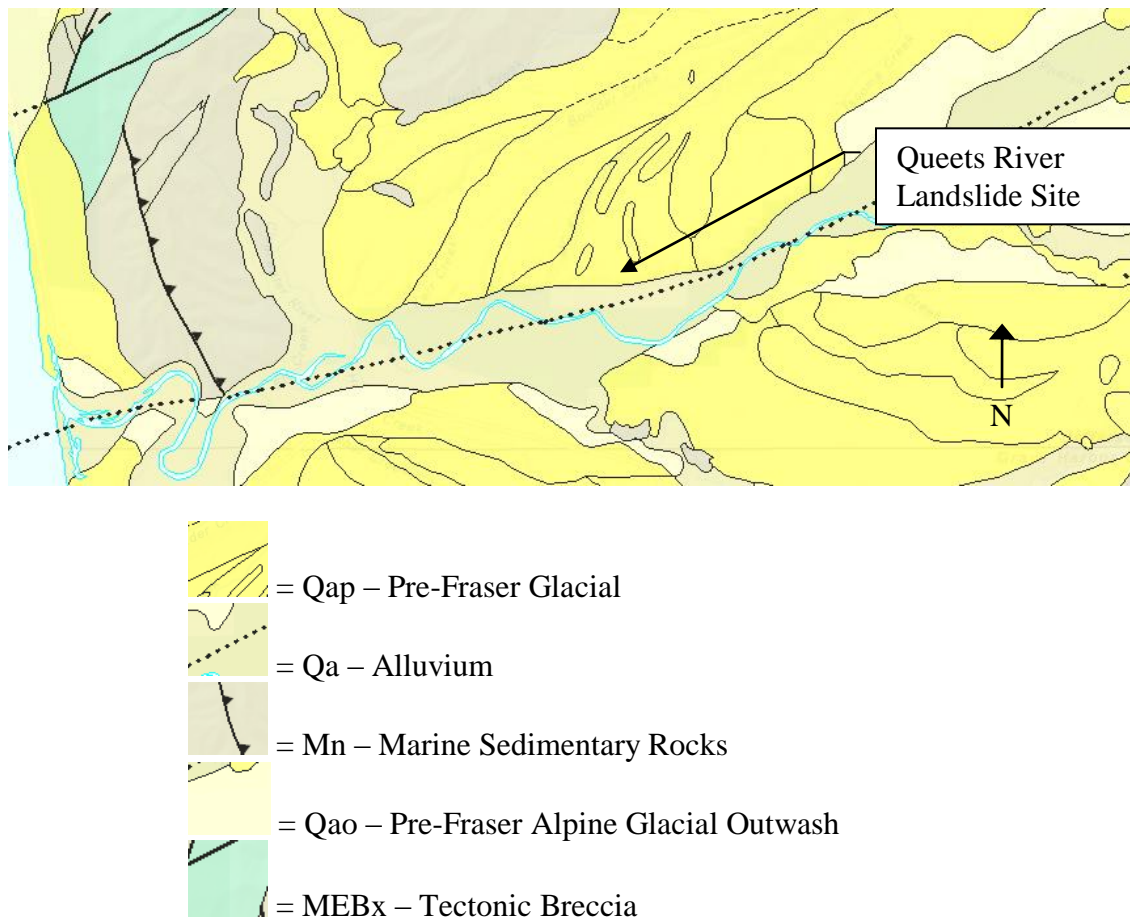
Figure 4-4: 1:100,000 scale geologic map of Queets River Landslide (Gerstel and

Lingley, 2000)

4.2.4 Subsurface conditions

Subsurface conditions are based upon the United States Department of

Agriculture (USDA) soil survey issued in Jefferson County in 1975 (McCreary and

Raver, 1975). The USDA Soil Survey documents typical soil characteristics for the

upper 150 centimeters (60 inches) of soil in the mapped region.

Based on the USDA Soil Survey the site is comprised of Klone Gravelly Silt

Loam, which is a glacial outwash and/or till material deposited in planes and terraces.

The soil is described as the following: being well drained; moderately high to high capacity to transmit water, 1.5 to 5 *cm/hr* (0.57-1.98 *in/hr*); low available water capacity, about 9.2 centimeters (3.6 inches); and no frequency of flooding or ponding. The soil profile is comprised of three layers in the top 150 centimeters (60 inches): from 0 to 18 centimeters (0-7 inches) a Gravelly Silt Loam, 18 to 91 centimeters (7-36 inches) a Very Gravelly Silt Loam, and 91 to 150 centimeters (36-60 inches) a Very Gravelly Loamy sand. Table 4-1 below shows the estimated properties of each of the materials that comprise the soil section.

Depth	USDA Texture	Classification		Percent Passing Sieve						Liquid Limit	Plasticity Index
		USCS	AASHTO	10"	3"	4	10	40	200		
0-18 cm 0-7"	Gravelly silt loam	OL, GM, MH, ML	A-5, A-7	100	100-85	60-80	50-70	45-65	35-60	40-60	5-25
18-91 cm 7"-36"	Very gravelly silt loam, Very gravelly loam, very gravelly sandy loam	GM, SM	A-2, A-5, A-7	100	90-80	45-75	35-50	25-50	20-45	40-60	5-25
91-150 cm 36"-60"	Very gravelly loamy sand, Extremely gravelly sand, very gravelly sandy loam	GP, GP-GM, SP, SP-SM	A-1	100-95	100-90	30-60	25-50	15-30	0-10	0-14	NP

Table 4-1: Klone Gravely Silt Loam Soil Properties (Jefferson County, 2009)

4.2.4.1 Cohesion

The upper 150 centimeters (60 inches) of soil has been classified as a silty

gravelly sand loam to gravelly loam; therefore, the cohesion can be assumed to be zero.

From the geologic setting of the failure, glacial outwash, it can be assumed that the soil is

not overly consolidated, which also leads to the assumption that the cohesion in the soil is

negligible. Cohesion is the parameter many engineers and geologist attempt to estimate

through back calculation of slope failure, resulting in a higher than actual value.

4.2.4.2 Soil friction angle

Typical soil friction angles of loose poorly graded sandy soils are between 27

degrees and 32 degrees (Bowles, 1995). The Friction angle assumed for this soil was 28

degrees. According to Gan et al (1988), compacted glacial till has a typical suction

friction angle range of 7 degrees to 25.5 degrees. While the outwash soil in this profile is

not a till, a suction friction angle near the lower end of the range seems reasonable for the

outwash present at the site. Therefore, the suction friction angle is assumed to be 10°

degrees.

4.2.4.3 Dry unit weight

According to the NAVFAC 7.01, typical soil unit weights for silty sands and

gravels are between 14 and 24 kN/m^3 (90-155 lb/ft^3). Based on the soil gradations in

Table 4-1, a lighter unit weight of 15.3 kN/m^3 was used for the two upper soil units, while

a heavier unit weight of 20.1 kN/m^3 was assumed for the lower soil unit, 91 to 150 centimeters (36-60 inches) in depth.

4.2.5 Vegetation

Based on a study of areal maps of the region, it appears that the site had been recently logged at the time of the landslides. The site naturally contained fir and spruce trees similar to what is found ¼ mile southwest in the Olympic National Park. Currently and at the time of the landslide, the site is a working fir and spruce tree farm.

For model validation analysis, an assumed clear-cut condition was used since the site had little to no vegetative cover during failure. However, additional soil strength due to roots was assumed since the roots were still present, but in a decaying state.

4.3 Clallam River Slope

The second landslide chosen for this study occurred upslope of a smaller tributary creek to the Clallam River in northern Clallam County which feeds into the Strait of Juan De Fuca. The site is on the Washington State Department of Natural Resources land and is used for timber harvest. The site slopes down to the north and is bound by an existing logging road both upslope and downslope. The site was located at an elevation of approximately 455 meters (1500 feet) above sea level in the foothills of the Olympic Range (Figures 4-5, 4-6, and 4-7).
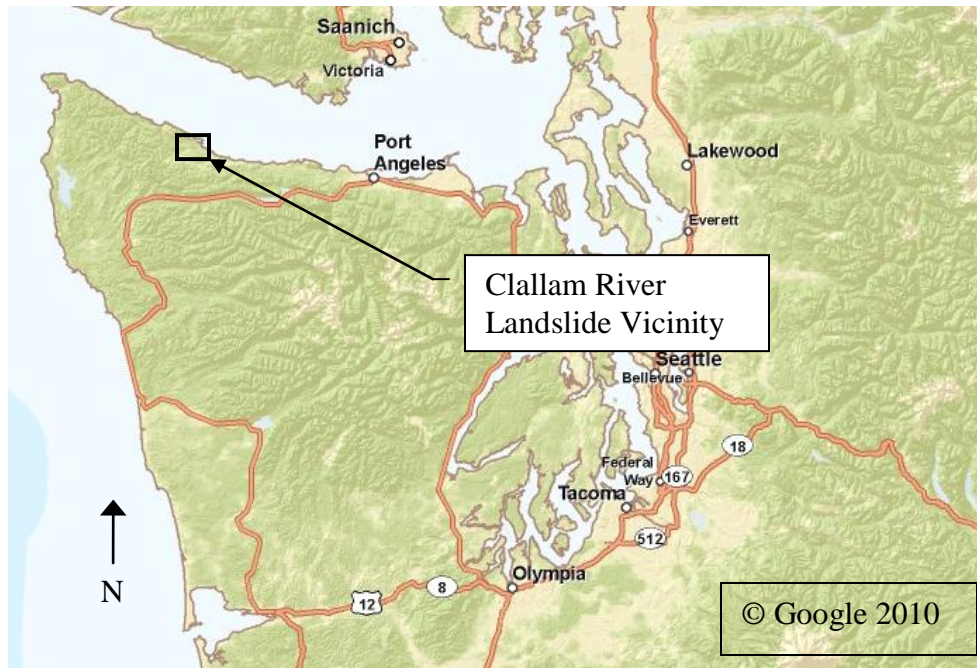
Figure 4-5: Vicinity map of Clallam River Landslide
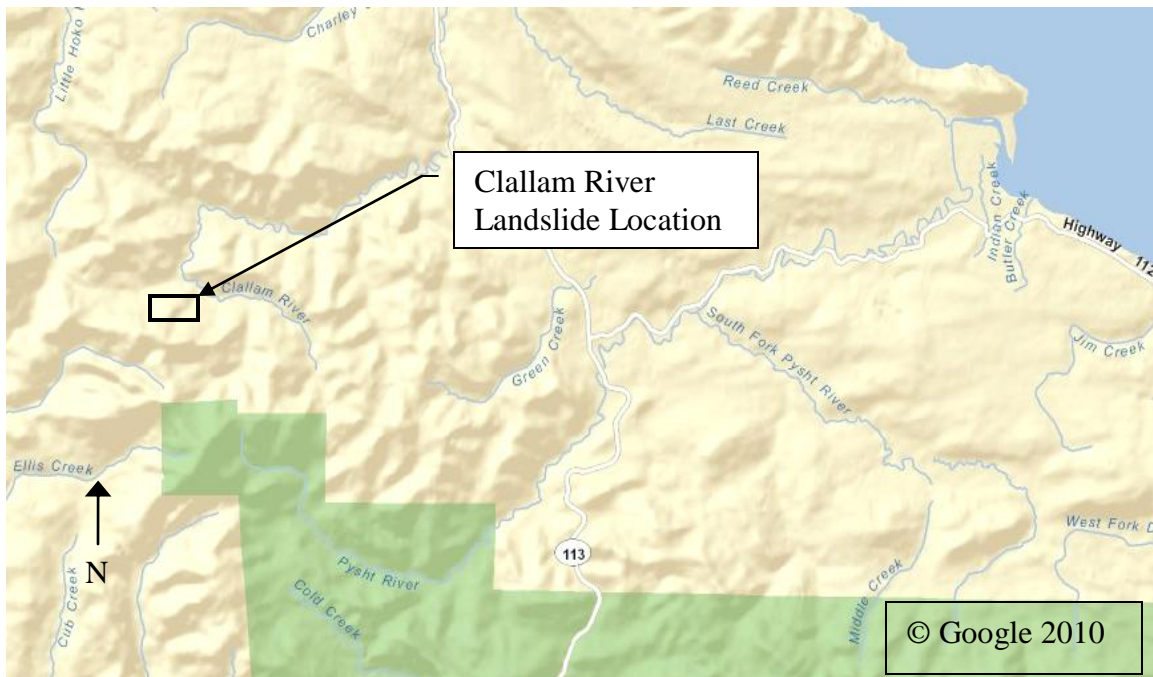
Figure 4-6: Site map of Clallam River Landslide
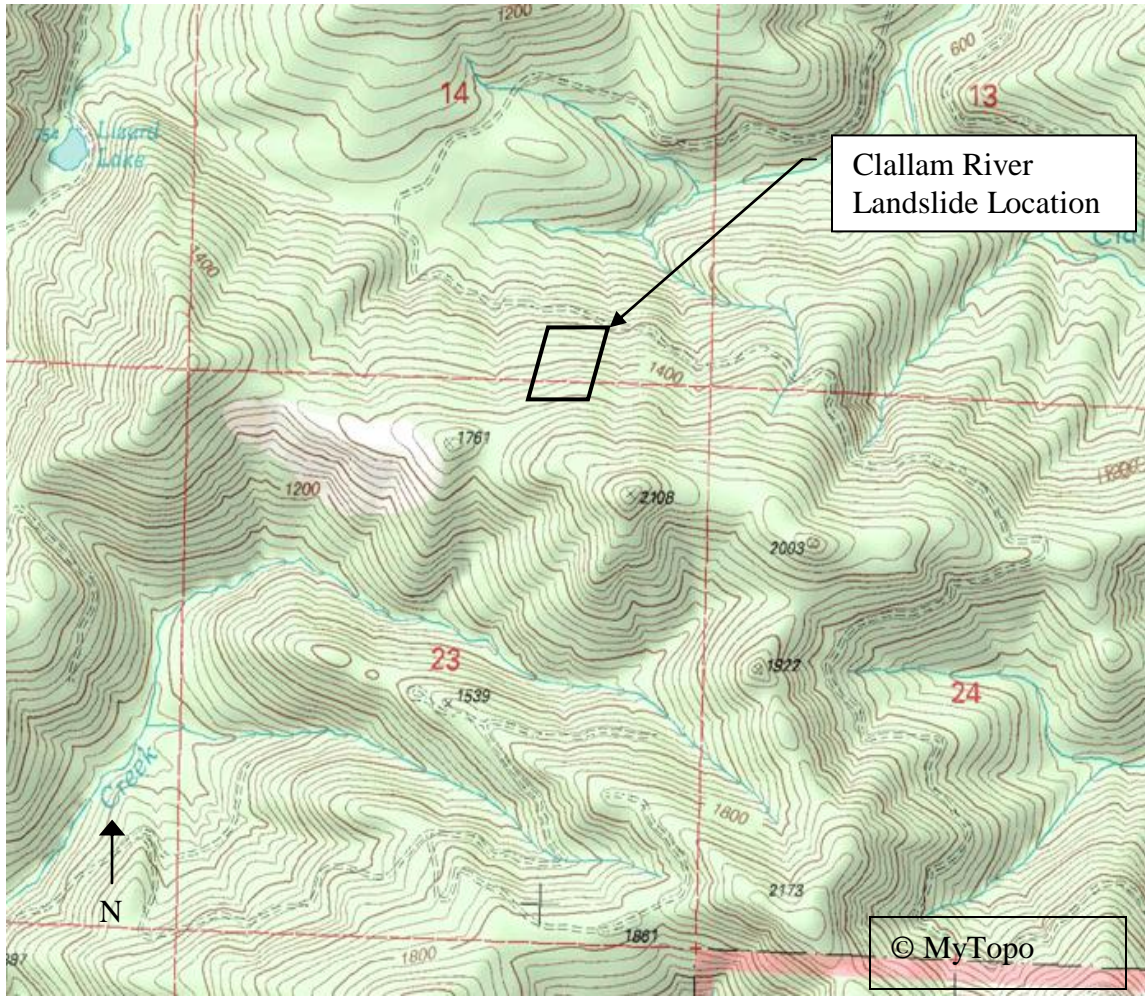
Figure 4-7: Topographical map of Clallam River Landslide

4.3.1 Landslide

Information on the landslide was determined from the landslide inventory associated with the Clallam River WAU Landslide Hazard Zonation Project Mass Wasting Assessment (Slaughter, 2007). The assessment classified the landslide as a shallow undifferentiated failure and is described as being a very shallow landslide. Under natural conditions this classification's dominant trigger mechanism is elevated pore water pressures associated with heavy rainfall events (Slaughter, 2007). However,

the landslide rate is moderately increased by logging operations including harvest and road building. The landslide at this site covered 6758 square meters (1.67) acres and had a height and lateral extent of approximately 97.5 meters (320 feet) (Slaughter, 2007).

4.3.2 Slope description

The north facing slope at the Clallam site slopes at a relatively constant steep slope of 1:1. The slope is bounded by two well established logging roads upslope and downslope that could have influenced the stability of the slope due to their proximity to the slide.

4.3.3 Local geology

Based on a review of geologic maps (Tabor and Cady, 1978 and Dragovich et al., 2002), the geology at the Clallam slide location is part of the Lower-middle Eocene Crescent Formation (Ev_c). The geology was formed 55 to 45 million years ago during the middle to early Eocene age of the Tertiary (Figure 4-8). The geologic unit is described with the following: tholeiitic basalt flows, basaltic flow breccias, filled tubes, and volcaniclastic conglomerate; gabbro dikes and sills; locally contained thin interbeds of basaltic tuff, chert, red argillite, limestone, and siltstone; rare andesite, dacite, and rhyolite; marine, pillow-dominated lower part grades into flow-dominated, partially non-marine near top with local columnar jointing; altered to palagonite, chlorite, zeolite, or epidote. The Lower-Middle Eocene Crecent formation consists of part of the Crescent Formation.
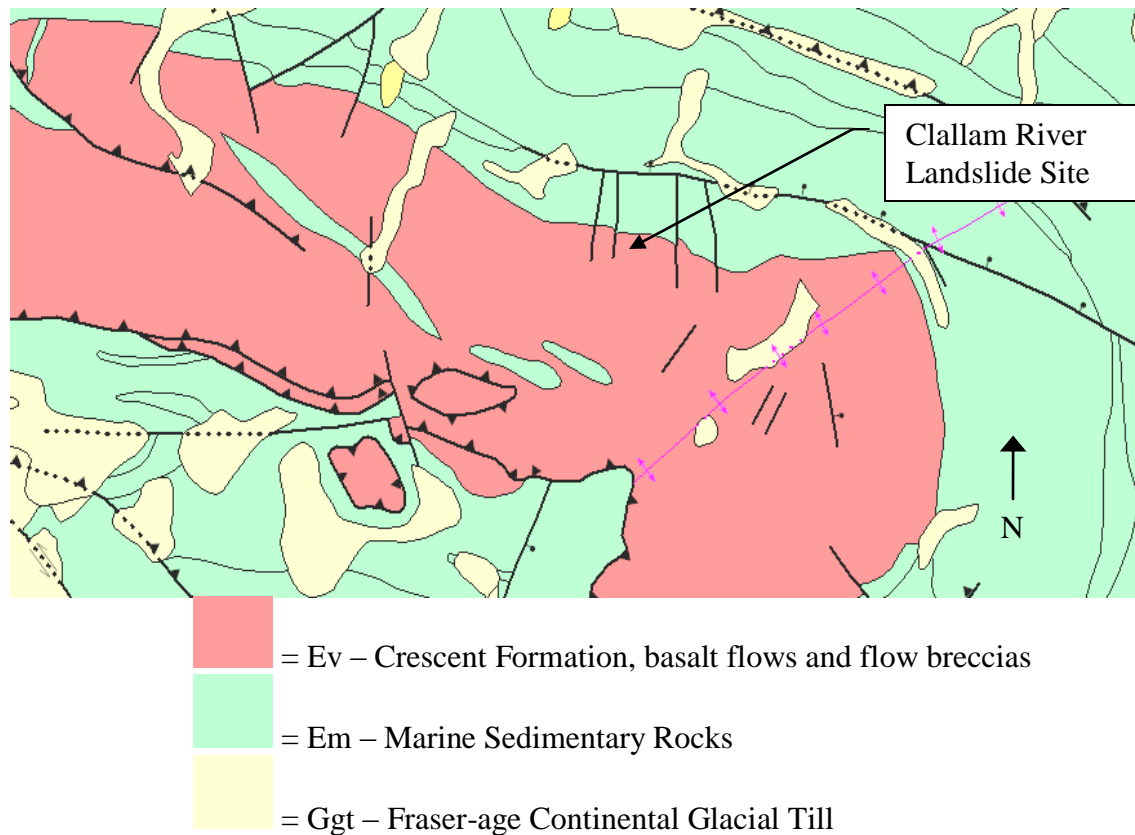
Figure 4-8: 1:100,000 scale geologic map of Clallam River Landslide (Tabor and Cady, 1978)

4.3.4 Subsurface conditions

Subsurface soil conditions at the site are based upon the USDA soil survey conducted in Clallam County in 1987 (Halloin et al., 1987). The USDA Soil Survey documents typical soil characteristics for the upper 150 centimeters (60 inches) of soil in the mapped region.

USDA Soil Survey indicates the site is comprised of Hyas Gravely Loam, which is described as colluvium and residuum derived from basalt and was in the form of mountain slopes (Halloin et al., 1987). The soil is described as the following: well

drained; moderately high to high capacity to transmit water, 1.5 to 5 *cm/hr* (0.57 to 1.98

in/hr); moderate available water capacity, 16.8 centimeters (about 6.6 inches); and no

frequency of flooding or ponding. The soil profile is comprised of three layers in the top

150 centimeters (60 inches): from 0 to 33 centimeters (0-13 inches) a Gravelly Loam, 33

to 97 centimeters (13-38 inches) a Gravelly Loam, and 97 to 150 centimeters (38-60

inches) a Very Gravelly Loam. Table 4-2 below shows the estimated properties of each

of the materials that comprise the soil section.

Depth	USDA Texture	Classification		Percent Passing Sieve						Liquid Limit	Placticity Index
		USCS	AASHTO	10"	3"	4	10	40	200		
0-13"	Gravelly loam	MH, ML, SM	A-5, A-7	100	100-90	70-85	60-75	50-70	35-55	40-60	5-20
13"-38"	Gravelly loam	GM, MH, ML, SM	A-2, A-5, A-7	100	100-90	65-85	55-75	45-70	30-55	40-60	5-20
38"-60"	Very gravelly loam, Gravelly loam	SM, GM	A-6, A-7, A-2, A-4	100	100-85	55-80	45-75	40-60	30-50	30-50	5-20

Table 4-2: Hyas Gravely Loam Soil Properties (Clallam County, 2009)

4.2.4.1 Cohesion

The upper 150 centimeters (60 inches) of soil has been classified as a gravelly

loam to very gravelly loam indicating soil with cohesion. From the geologic setting of

the failure, weathered basalt, it can be assumed that the soil is not overly consolidated,

contributing to typical soil cohesion values. Typical cohesion values of weathered basalt

are 0 to 5 *kPa*. For this analysis, a value of 4.5 *kPa* was chosen due to the indication

from sieve data displayed in Table 4-2 of gravelly soils. Therefore, the basalt has not undergone extensive weathering reducing the cohesion of the soil.

4.2.4.2 Soil friction angle

Typical soil friction angles of weathered basalt are between 27 degrees and 35 degrees. The friction angle assumed for this soil was 31 degrees.

4.2.4.3 Dry unit weight

According to the NAVFAC 7.01, typical soil unit weights for silty sands and gravels are between 18 and 24 kN/m^3 (115-151 lb/ft^3). Based on the soil gradations in Table 4-1, a unit weight of 18.9 kN/m^3 was used for the soil profile.

4.3.5 Vegetation

The arial photos used for this study indicated that the slope had young, (i.e., 10-15 year old) trees when the slope failure occurred. Naturally, the site was densely forested with fir and spruce trees. At the time of the slide, the site was used as a tree farm, and was likely to have been clear cut within the past 20 years.

For analysis, partial rainfall interception by the vegetation was assumed. Little influence from the root system was assumed, since many of the roots were not fully developed at the time of failure.

4.4 Rainfall

Rainfall data from the December 2007 storm, which caused many landslides to occur in the Olympic Region, was used for validation of the model analysis. Although the landslides studied did not occur during this storm – the Clallam slide was discovered in 1977 and the Queets slide was discovered in 1985 – the exact time and date of the landslides are unknown. It can be assumed that if the same vegetation conditions were present on the study slopes in 2007, the December 2007 rainfall would have caused failure.

The hourly rainfall data from the December 2007 storm is presented in Figure 4-9 (NOAA, 2009). The rainfall data was collected from a weather station located in Forks, Washington and record hourly rainfall data to the nearest 2 millimeter during the December 2007 storm. The hourly data indicates that the storm event had very heavy rainfall from hour 20 to approximately hour 35 with the maximum rainfall in a one hour period reaching 12.7 mm. As the storm event continued beyond the 55th hour, the rainfall intensity reduced to nearly zero.
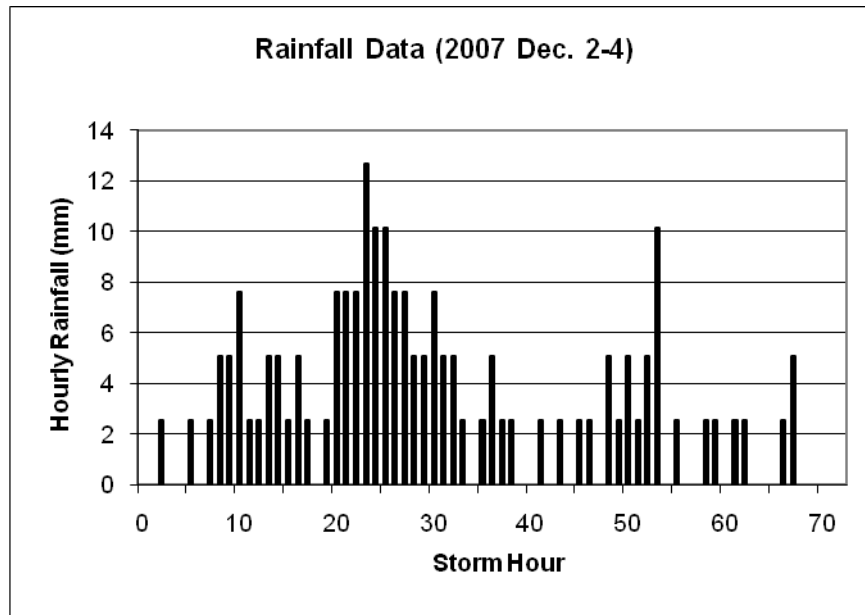
Figure 4-9: December 2007 storm hourly rainfall intensity

Cumulative rainfall amounts are also very important in estimating soil moisture contents during a storm event, since factors such as vegetation interception and soil hydraulic conductivity mute the effects of peaks in rainfall intensity. The cumulative rainfall for the December 2007 storm is illustrated in Figure 4-10. The figure illustrates that, over the 72 hour period of the storm, a total of 229 millimeters of rainfall was recorded.
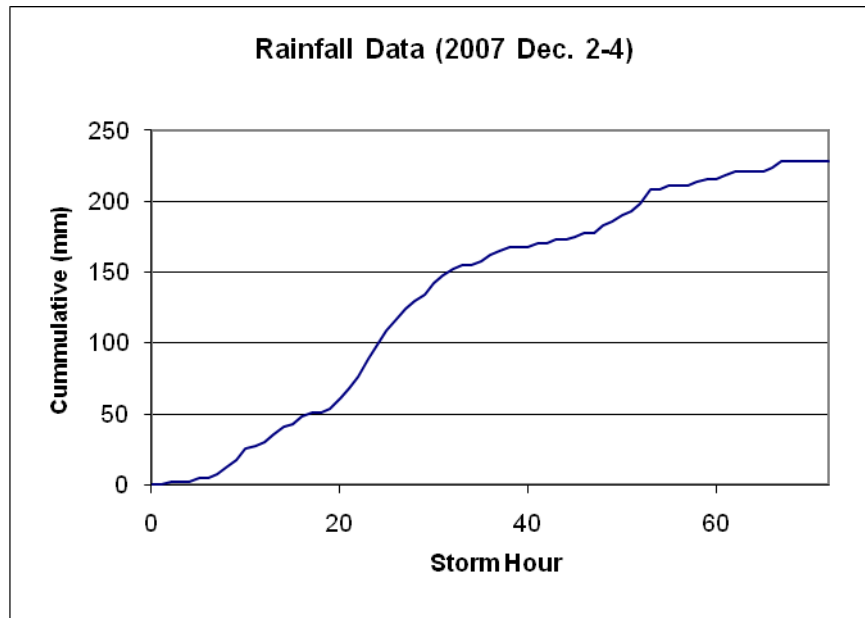
Figure 4-10: December 2007 storm cumulative rainfall

4.5 Queets Failure Analysis

To illustrate how the model works and the decision process was used to determine the stability of slopes, an example of the Queets slope at the 24th storm hour is presented first. The process of modeling involves output of the hydrologic model as input data into the slope stability model with suction developed in Chapter 3.

4.5.1 Hydrologic model input

Proper account of the hydrologic conditions of the slope is possibly the most important aspect of the modeling process. This model makes use of CHASM's hydraulic modeling capabilities to account for proper estimation of groundwater conditions and soil suction. The main page interface of the combined hydrologic and slope stability program, CHASM, is presented in Figure 4-11
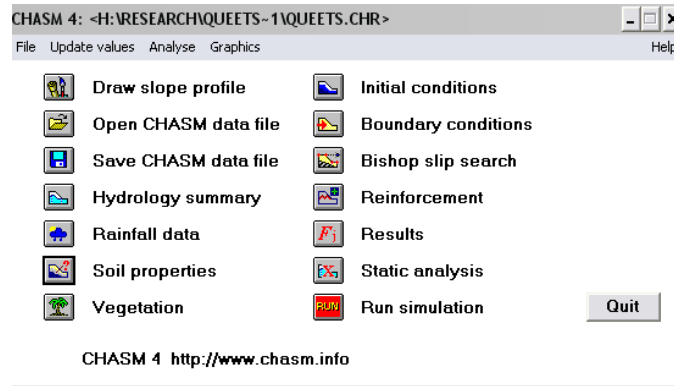
Figure 4-11: CHASM main page interface

The process starts by setting up the proper geometry of the slope (Figure 4-12). A slope of 1.28:1 was selected for analysis of the Queets slope. The details of the slope geometry selection and reasoning are presented in Section 4.2.2. Note that CHASM only evaluates slope failures from left to right and that CHASM is based in SI units.
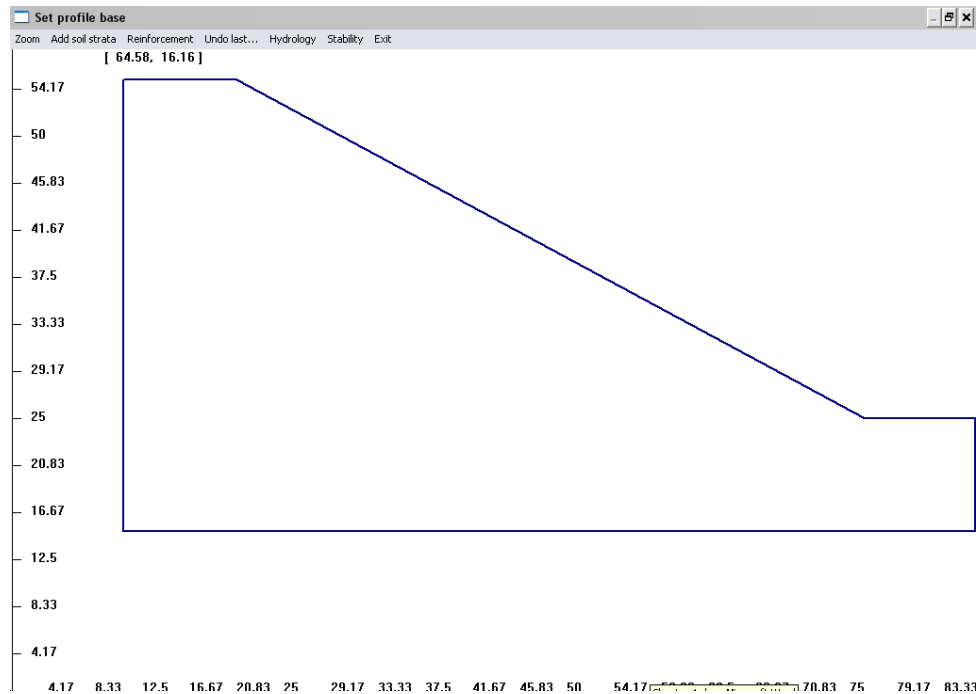
Figure 4-12: Queets example slope geometry (meter units)

Next, the soil depths and grid resolution are selected. It is important to select soil depths that are similar to the grid resolution. CHASM recommends a grid resolution of 1-meter by 1-meter (Wilkinson et al. 2002). For the Queets Slope, the soil profile presented in Section 4.2.4 was simplified into two soil layers to allow for proper grid resolution. Because CHASM only evaluates slopes with a flat bottom, a third soil layer was selected for the lower elevations shown in Figure 4-13.

Figure 4-13: Queets example soil profile (meter units)

If the CHASM slope stability capabilities were to be used in the analysis a slip surface search grid would be selected at this point. However, in the study, here on shallow slides, infinite slope stability is more appropriate and as such the selection of slip surface search grid location is ignored.

Once the slope geometry was established, the soil parameters were input for each soil type. Because only the hydrologic modeling capabilities of CHASM were being

used, the hydrologic properties were the only properties that were of importance. Saturated moisture content and saturated hydraulic conductivity as discussed in Section 4.2.4, were used for the analysis. Figure 4-14 is an image of CHASM's soil property window. By selecting the Suction Moisture Relationship button on the soil property window, the soil suction window (Figure 4-15) is opened allowing the input of points along the soil suction curve.
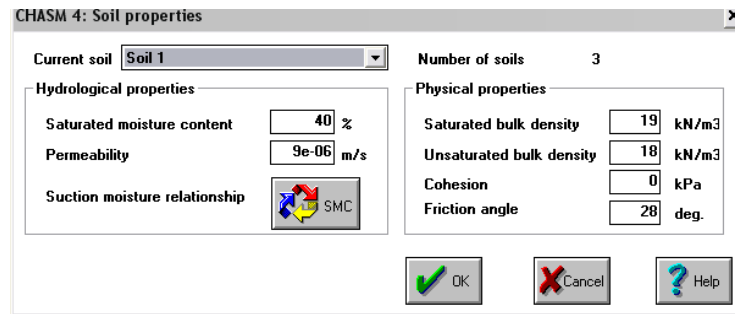
Figure 4-14: CHASM soil property interface
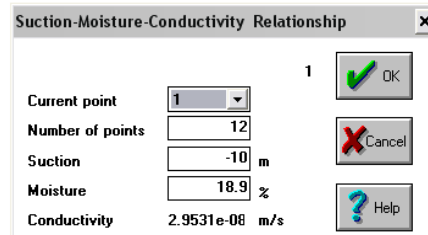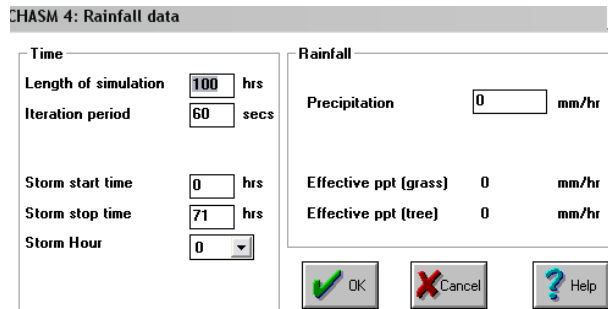
Figure 4-15: CHASM suction interface

Next, the rainfall data from the December 2007 storm event in units of meters for each hour of the storm was input for the rainfall data. See Figure 4-9 for hourly data. The analysis was run for 100 hours even though the rainfall data was only collected for 72 hours. Further discussion on rainfall data selection is presented in Section 4-4. Rainfall data was entered into CHASM by entering the precipitation for each hour of the simulation in the Rain Fall Data window (Figure 4-16).
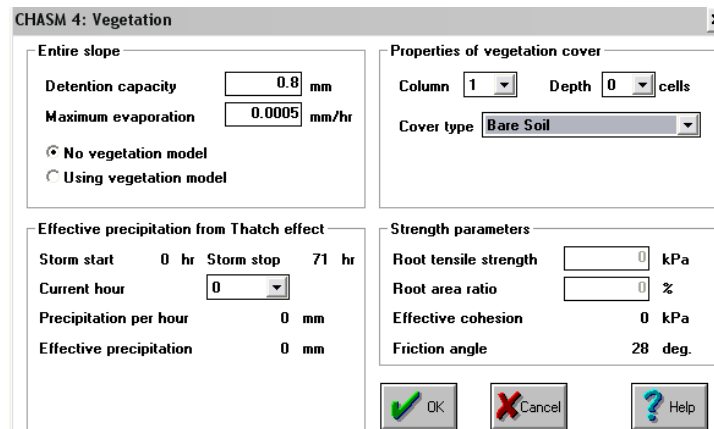
Figure 4-16: CHASM rainfall input interface

As discussed in section 4.2.5, no vegetative cover was assumed for the Queets slope. However, if vegetative cover is desired, such information can be input by selecting the user defined tree option in CHASM and inputting the proper detention capacity and evaporation for the vegetation selected. For this analysis, the bare soil option was selected. Figure 4-17 shows CHASM's vegetation input window.

Figure 4-17: CHASM vegetation input interface

When all the hydrology data was input into CHASM, the model was run by selecting the "Run Simulation" on the main page (Figure 4-11). The slope output information was of no relevance here since a separate infinite slope analysis was to be evaluated. However, hydrologic output of interest was the hydrograph which can be obtained from the CHASM main page (Figure 4-11). Once the hydrograph was opened

(Figure 4-18), the storm hour of interest was selected, for this example the 24th hour. A column near the center of the slope, column 30, was selected to represent the soil moisture and pore pressure within the slope.
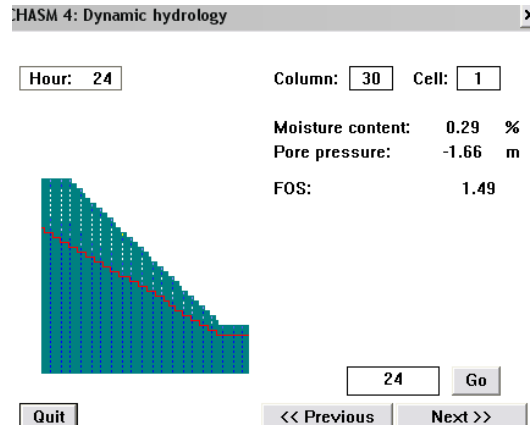
Figure 4-18: Queets example hydraulic output

Table 4-3 presents the water content and pore pressures for each of the cells in column 30. Note that the cell numbers correlate to the cell depth since a 1-meter by 1-meter cell dimension was selected. Based on the discussion in Section 2-1, the pore pressures presented in Table 4-3 were used to determine the soil suction values used in the infinite slope stability model.

Column 30 @24hr		
Cell Number	Water Content (%)	Pore Pressure (m)
1	29	-1.66
2	20	-2
3	3	-2
4	3	-2
5	3	-2
6	3	-2
7	2	-2
8	5	-1.27
9	12	-0.29
10	20	0.5

Table 4-3: Queets Example Hydrologic Table from Output

4.5.2 Analysis of slope stability

After the water content and pore water pressures were accurately determined from the hydrologic model, the infinite stability model described in Chapter 3 was analyzed to determine the stability of the slope.

$$FOS = \frac{c'_s + c'_R + \cos^2(\beta)[(\Sigma \gamma_m D_c) + S_w]\tan\phi' + (u_a - u_w)\tan\phi^b}{\sin(\beta)\cos(\beta)[(\Sigma \gamma_m D_c) + S_w]} \qquad (3\text{-}30)$$

The relevant parameters for this model are listed below.

- Soil Cohesion: $c'_s = 0$, See section 4.2.4.1

- Root Effect: $c'_R = \dfrac{\sigma_R}{2\sqrt{K_a}} = \dfrac{0.4}{2\sqrt{0.36}} = 0.33$;

  - Root Strength: $\sigma_R = T_R\left(\dfrac{A_R}{A}\right) = 20\left(\dfrac{0.02}{1}\right) = 0.4$;

  - Tensile Stress: $T_R = 20KN/m^2$, for very weak decaying Fir and Spruce-Hemlock roots (Burroughs and Thomas, 1976; Gray, 1978; and Turmanina, 1965);

  - Area of Roots: $A_R = 0.02m^2$, from a study that measured root density by excavating test pits and measuring the roots of Hemlock and Sitka Spruce trees in the Maybeso Valley (Wu, 1976);

  - Unit Area: $A = 1m^2$;

  - Active Earth Pressure Coefficient:

  $$K_a = \tan^2(45 - \frac{\phi}{2}) = \tan^2(45° - \frac{28°}{2}) = 0.36;$$

- Slope Angle: $\beta = 38°$, the slope angle correlating to a slope of 1.28:1 is 38˚;

- Weight of Slice: $\Sigma \gamma_m D_c = \gamma_d (1 + \omega) = 15.3(1 + 0.29) = 19.7 kN/m^3$;

  o Depth of Failure: Queets failure was assumed to occur at a depth of approximately 1 meter; therefore, no summation is needed and the weight of the slice is only the weight of one cell;

  o Dry Unit Weight: $\gamma_d = 15.3 kN/m^3$, See section 4.2.4.3;

  o Moisture content: $\omega = 29\%$, See Table 4-3;

- Surcharge: $S_w = 0$, assumes clear cut condition with no additional weight due to trees;

- Soil Friction Angle: $\phi = 28°$, See section 4.2.4.2;

- Air Pressure at Slip: $u_a = 0$, assumes that no abnormal air pressures occur at the failure surface at the time of failure;

- Pore Water Pressure: $u_w = depth * 9.81 = -1.66m * 9.81 = -16.28 kN/m^2$, See Table 4-3 for depth;

- Suction Friction angle: $\phi^b = 10°$, For sandy soils.

Therefore, the driving forces on the slope are

$$= \sin(\beta)\cos(\beta)[(\Sigma \gamma_m D_c) + S_w] = \sin(38)\cos(38)[(19.7) + 0] = 9.58.$$

The resisting forces are

$$= c_s' + c_R' + \cos^2(\beta)[(\Sigma \gamma_m D_c) + S_w] \tan \phi' + (u_a - u_w) \tan \phi^b$$

$$= 0 + 0.33 + \cos^2(38)[(19.7) + 0] \tan 28 + (0 - (-16.28)) \tan 10 = 9.60$$

The resulting factor of safety $= \dfrac{9.60}{9.58} = 1.002$, Which is only slightly above one. The

factor of safety of the slope fell below one, predicting a slope failure at 25 hours.

Therefore, the slope is stable for this example but should be close to failure with further

reduction in soil suction.

4.6 Results

In previous analysis of slope stability that ignored soil suction, it was assumed

that the soil would have to reach saturation before it would become unstable, which is

accurate if the friction angle of the soil is above the slope angle or soil suction is not

present in the soil. In many situations, this is not the case, so analysts have assumed a

higher than actual friction angle in an attempt to explain how a slope is stable when

traditional analyses show instability. The analysis conducted shows that soil suction has

a considerable effect on the stability of a slope, and if that soil suction is reduced, the

slope has the potential of becoming instable.

Based on the soil, slope, and rainfall conditions presented previously, the factor of

safety for the Queets River Landslides slope fell below 1, indicating slope instability

prior to reaching saturation at the failure plane. The idealized Queets river slope reached

a minimum stability at hour 25 during the storm when the rainfall was near its peak

intensity. According to the analysis, the slope failed at a depth of 1 meter which was the

contact between the surficial soils and the underlying soil with a higher infiltration rate.

As seen in Figure 4-19, if the slope had not failed at hour 25, the slope would have

quickly returned to a factor of safety above 1, due to the high infiltration rate of the
underlying soils.

Queets Factors of Safety During Storm
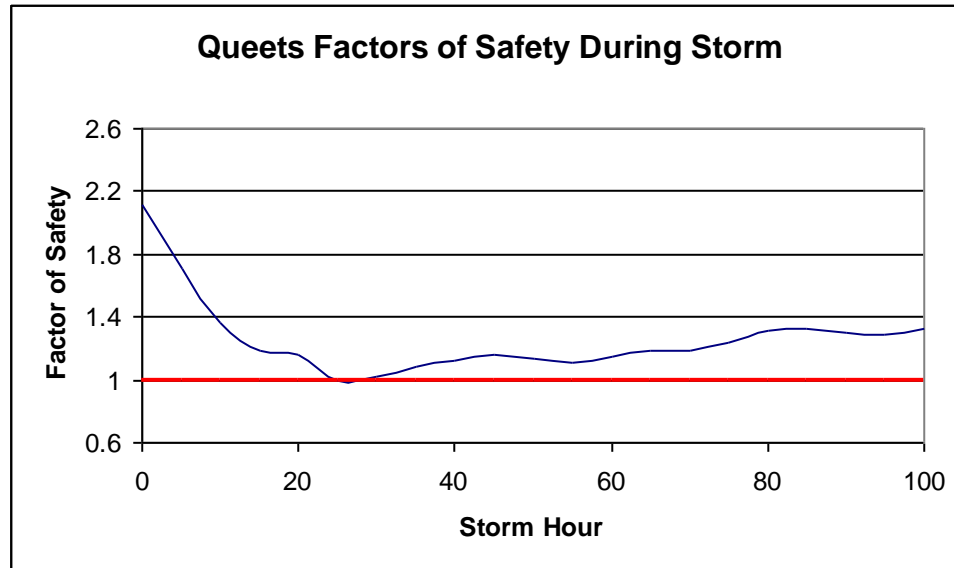
Figure 4-19: Factors of safety for December 2007 storm Queets River Landslide

Using similar analysis techniques as the Queets River Landslides, the Clallam
River idealized slope also reached an unsafe factor of safety below 1 before the soil
reached saturation. The factor of safety for the Clallam slope did not fall below 1 until
after the storm rainfall was complete. The model was continued an additional 29 hours
due to the soil suction continuing to drop after the 72-hour storm had completed. As is
illustrated in Figure 4-20, the factor of safety takes some time to drop below 1 and then
also did not return to a safe factor of safety immediately as the Queets river slope did.
This is likely due to the slower infiltration rate of the underlying soil. The water did not
return to its typical level until well after the intense rainfall had ended.

Clallam Factors of Safety During Storm
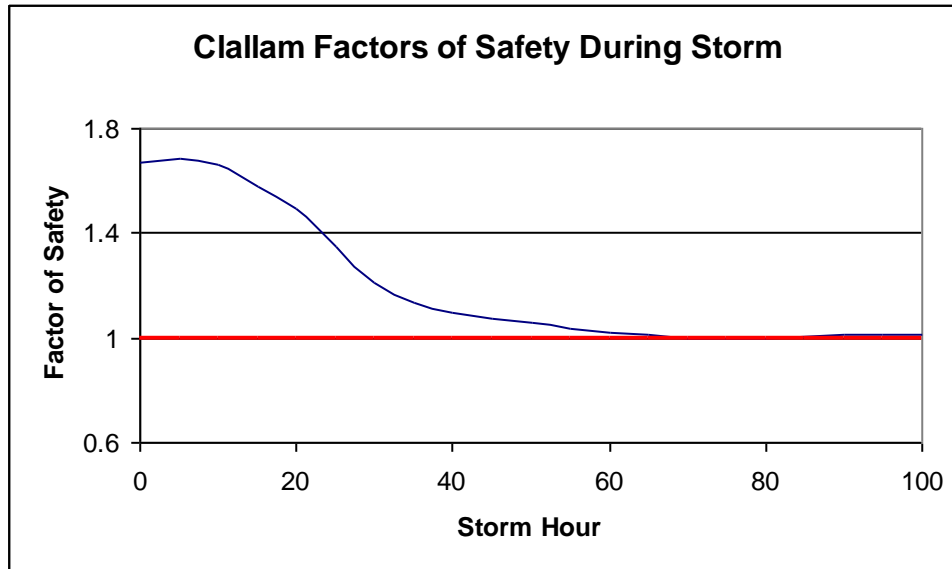
Figure 4-20: Factors of safety for December 2007 storm Clallam River Landslide

By using the two different slopes, it is evident that the soil suction affects different soil types differently, but it was still shown that soil suction had a significant influence on the stability of the slope. The Clallam slope appears to be more greatly affected by a long term rainfall event than the Queets slope, which would be affected more by a short, very intense rainfall event. This is likely due to the infiltration rates of the underlying soils and the soil suction at the failure plane.

CHAPTER 5

DESIGN CHARTS

5.1 Stability Charts

The model developed and verified was used to develop design charts that can be of use to engineers and land management personnel. The design charts presented in this chapter were developed for use as a general guideline for slope stability in the Olympic region of Washington State using generalized slope, vegetation, and rainfall data. The intended purpose of the charts is to give land management personnel an efficient way to determine if a particular slope is reaching a critical soil moisture condition under unsaturated conditions.

The proper way to utilize the following charts (Table 5-1 and 5-2) is to select a slope angle and then follow the column down until the appropriate number of years since harvest is reached. The number in this correlating box should be the critical amount of rainfall in a particular 24-hour period that would cause a factor of safety to be unity and cause slope failure. For example, if there was a slope in the Klone Gravelly Silt Loam with a slope angle of 40 degrees 20 years after a timber harvest, the rainfall for a 24-hour period that could cause slope failures under unsaturated conditions would be 252-milimeters (9.9-inches).

Klone Gravelly Silt Loam					
Rainfall Intensity for failure mm/24-hr *(in/24-hr)*		Slope				
		30	**35**	**40**	**45**	**50**
Vegetation years since harvest	**0**	*	768 *(30.2)*	216 *(8.5)*	84 *(3.3)*	30 *(1.2)*
	10	1200 *(47.2)*	540 *(21.3)*	150 *(5.9)*	45 *(1.8)*	15 *(0.6)*
	20	3150 *(124.0)*	840 *(33.1)*	252 *(9.9)*	84 *(3.3)*	21 *(0.8)*
	30	*	1188 *(46.8)*	324 *(12.8)*	108 *(4.3)*	41 *(1.6)*
	40	*	1872 *(73.7)*	504 *(19.8)*	180 *(7.1)*	72 *(2.8)*

* = slopes that were stable under unsaturated conditions

Table 5-1: Klone Gravelly Silt Loam Slope Chart

Table 5-2 for the Hyas Gravelly Loam can be utilized in the same way as Table 5-1. For

example, a slope with a slope angle of 60 degrees immediately after harvest would reach

unity and slope failure with a rainfall of 67-milimeters (2.6-inches) in a 24-hour period.

Hyas Gravelly Loam					
Rainfall Intensity for failure mm/24-hr *(in/24-hr)*		Slope				
		40	**45**	**50**	**55**	**60**
Vegetation years since harvest	**0**	312 *(12.3)*	127 *(5.0)*	86.4 *(3.4)*	72 *(2.8)*	67 *(2.6)*
	10	271 *(13.8)*	108 *(4.3)*	76.8 *(3.0)*	62.4 *(2.5)*	58 *(2.3)*
	20	351 *(13.8)*	141 *(5.6)*	99 *(3.9)*	81 *(3.2)*	75 *(3.0)*
	30	428 *(16.9)*	173 *(6.8)*	118.8 *(4.7)*	101 *(4.0)*	94 *(3.7)*
	40	576 *(22.7)*	240 *(9.4)*	163.2 *(6.4)*	134 *(5.3)*	125 *(4.9)*

Table 5-2: Hyas Gravelly Loam Slope Chart

Many of the parameters (soil properties, soil depths, suction curves, etc.)

established in Sections 4.2 and 4.3 for the two soil profiles were utilized to create

additional design charts. The design charts show variation in the slope angle, vegetative

cover, root density, vegetative surcharge, and rainfall as to illustrate a maximum

cumulative rainfall for a 24-hour period. Various slope angles and vegetation properties

were chosen to run in the model. By varying the rainfall intensity for a 24-hour period,

the maximum rainfall amounts for 24-hour periods were found to maintain a slope factor of safety above 1.0.

The following is a summary of the methods used to determine the applicable parameter variables used in developing Tables 5.1 and 5.2.

5.2 Slope Ranges

Typical slope ranges for the two soils used in the model validation of Sections 4.2 and 4.3 were selected in 5 degree increments to establish a generalized design chart. According to the USGS soil survey of Jefferson County in 2009, the Klone Gravelly silt loam, the soil used in the Queets River failure validation, and similar soils are found on slopes ranging from 0 to 90 degrees. For the purpose of the chart development, only slopes ranging from 30 to 50 degrees were evaluated due to the low probability of failures occurring on slopes less than 30 degrees and large variations in soil properties for slopes over 50 degrees. The Hyas Gravelly loam, soil used in the Clallam River validation, and similar soils are found on slopes ranging from 30 to 90 degrees. Hyas slopes ranging from 40 to 60 degrees were evaluated, due to the higher influence of soil moisture on slopes in this range of slope angles.

5.3 Vegetation Conditions

The chart assumes slope vegetation to be managed timber lands with clear-cut harvest intervals of 40 to 50 years. However, the chart could also be used in unmanaged timberlands for the first 40 years after a forest fire where native trees have been replanted and typical managed timberland vegetative cover and root densities are maintained. An

average root density and cover from Douglas Fir, Western Hemlock, and Spruce at ages of 0, 10, 20, 30, and 40 years were input into the model to determine the critical soil moisture for the various ranges of slope angles.

5.4 Root Density

According to Wu (1976) the typical root cross sectional area for the upper two meters of soil for a fully developed Western Hemlock and Douglas Fir forest is approximately 5 percent of the total cross sectional area. When timber land is harvested, the root structure and strength remains until the roots begin to decompose. Therefore, the root strength and cross sectional area at 0 years was modeled the same as at 40 years (5% root area). At 10 years, the root system of the new growth has not fully developed, and the strength of the existing roots has begun to decline due to rot (2% effective root area). At 20 to 30 years the new growth root system is developing, thereby increasing the root effect (3% and 4% root area respectively).

5.5 Vegetative Cover

A fully developed forest significantly reduces the amount of rainfall reaching the soil and infiltrating into the soil due to evaporation and evapotranspiration. The heavy vegetative cover assumed for the 40 year growth was designed to intercept approximately 2/3 of the rainfall prior to reaching the soil.   No reduction in rainfall was modeled in the slopes immediately after timber harvest since no vegetative cover was present, assuming clear cut timber harvesting techniques were conducted.

5.6 Surcharge

As timber matures, an added weight is added to the surface or near surface of the soil. Costal forest types of the Pacific Northwest have surcharges ranging from 1 to 5 *kPa* for mature forests (Bishop and Stevens (1964), O'Lloughlin (1974), Wu et al. (1979)). For the purpose of developing the design chart, an assumed surcharge at 40 years was 2 *kPa* due to the weight of the trees on the slope. Another assumption made for the chart development was that the surcharge increases linearly from 10 to 40 years. No surcharge was assumed for immediately after harvest since no trees would be present on the slope.

5.7 Rainfall Events

The method used to create the charts was to input the appropriate slope and vegetation parameters into the model and then vary the rainfall intensity for a 24 hour period until the factor of safety for the slope became one. The units of rainfall intensity input into CHASM are *mm/hr*. Therefore, a constant intensity for the 24-hour period was used.

5.8 Design Chart Results

The design rainfall for 2, 10, 25, 50, 100, and 500 year storms over a 24-hour period for the two validation slopes in Sections 4.2 and 4.3 were determined using USGS's stream stats runoff estimations. Table 5.3 presents the findings in inches per 24 hour period according to the USGS stream stats (Ries III, 2008).

mm/24-hr *(in./24-hr)*		Slope Location	
		Queets River	Clallam River
Storm Interval	2-yr	54.2 *(2.13)*	*7.4 (0.29)*
	10-yr	85.2 *(3.35)*	13.1 *(0.51)*
	25-yr	100.0 *(3.94)*	16.1 *(0.63)*
	50-yr	113.0 *(4.45)*	18.7 *(0.74)*
	100-yr	126.1 *(4.97)*	20.9 *(0.82)*
	500-yr	158.3 *(6.23)*	27.1 *(1.07)*

Table 5-3: Design Storm Rainfall Amounts (Ries III, 2008)

Interestingly the rainfall intensities illustrated in Table 5.3 show that thoose near the Clallam River location are expected to be much lower than those found at the Queets River location. The Queets region is known for having the heaviest rainfall recorded in a 24 hour period in the state at 305-milimeters (12-inches) in 1935. This indicates both that the critical rainfall intensities are more likely to be reached in the Queets region than in the Clallam region, and that a single storm event over 305-millimeters (12-inches) in a 24-hour period is very unlikely. Therefore, slope angles less than approximately 40 degrees for both soils can be assumed to be safe. Another assumption that can be made from correlating the design chart and design rainfall amounts is that slopes of 50 percent and steeper in the Queets region without full vegetation would likely see rainfall events exceeding the amount that would cause instability approximately every 2-years. This assumption can be made because rainfall events of 54.2 mm/24-hr (2.13 in/24-hr) is expected every 2-years, and an event of this magnitude would likely cause instability according to the design chart for slopes without full vegetative cover.

CHAPTER 6

CONCLUSIONS AND RECOMMENDATIONS

6.1 Discussion

This study presented a combined hydrological and slope stability method of analyzing the stability of slopes in an unsaturated condition. The analysis was developed using the hydrological modeling capabilities of the stability program CHASM and the infinite slope limit equilibrium equations with the added feature of soil suction. Commonly used stability analysis methods have not included soil suction or hydrologic models.

Utilizing a hydrologic model for determining soil moisture conditions allows engineers to account for vegetation and soil suction which had typically been ignored in other analyses. It is important to take soil suction into consideration as it plays a significant role in shallow failures. In order to estimate soil properties, the typical method is to back-calculate the soil properties using a slope that is near failure. If soil suction and pore water pressure above the phreatic surface is not taken in consideration, the soil properties that are estimated are very conservative. Many times, the soil properties used in analysis do not match the soil properties determined by laboratory analysis since conservative soil properties are determined in back calculations. By taking soil suction into consideration during the model validation/soil property determination, engineers can determine the appropriate soil properties and consequently the proper stability factors for the desired slope. As shown in this study, the model presented can properly predict a slope failure under an actual intense rainfall event.

While the methods used in this study are not as simple and streamlined as many other methods that are commonly used in engineering, this study presents a few important factors that affect slope stability in the Olympic region of Washington State: (1) planar failure surfaces are very common in the Olympic region; (2) the Olympic region has a unique situation in that many of the slope failures are not due to roadway or transportation cuts into the slope but, rather, the change in vegetation due to timber harvesting; and (3) very heavy rainfall is common to the region. The methods presented could be used to more accurately model the slope stability in the Olympic region since the features that are unique to the region may be included.

Chapter 5 presented a design chart that can be used by engineers and land management personnel to easily determine the critical rainfall event for a particular slope angle and vegetation condition. The design charts were developed using the hydrological modeling capabilities of the stability program CHASM and the infinite slope limit equilibrium equations with the added feature of soil suction as was used for the model validation for two regions within the OESF presented in Chapter 4. The design charts should give land management personnel, who have to analyze many slopes over a large area, an easy way accurately predict the potential for slope failure.

6.2 Recommendations

This study was developed to properly model the mechanics of failure of particular slopes. The most effective use of this model is to select a certain slope or multiple slopes with similar soil profiles and run the model with varying vegetation properties against predicted storm events.   The model is useful to forest land managers to better predict

when a failure may occur on a particular slope so that failure can be mitigated with stability enhancing procedures or timber harvest techniques.

The model should not be used for widespread stability predictions across multiple slope profiles. Chapter 5-1 presented design charts for particular soils that may be very useful when evaluating the stability of multiple slopes within a similar soil profile since it is very easy to read and understand. However, due to the variations in soil profiles, a design table created for one area with in the Olympic region should not be used in another area without careful consideration.

6.3 Further Studies

As is the case with any new method for determining slope stability, it is important to validate the analysis in the field. Multiple slope failures should be carefully analyzed and back-calculated to ensure that the model is appropriate for use in the Olympic region. To properly validate the model for the use in the region, a failure would need to occur on a heavily instrumented slope with frequently read piezometers and rainfall gauges at the soil surface. The peizometers would allow for proper determination of water level at the time of failure and the rain gauges would show the amount of rainfall that is reaching and infiltrating into the slope soil. As discussed in Section 2.2.1, a study has been conducted on a heavily instrumented slope in the Seattle area of Washington that properly validated the use of a similar infinite stability and suction model. However, the study did not include hydrological effects (Lu and Godt, 2008).

Until enough data is collected in the region to validate the model, it is important to use it with caution. To reduce the level of uncertainty for a particular slope, the

installation of rain gauges at the surface and peizometers could be used to determine how rainfall events measured at a nearby rain station affect the soil moisture conditions in the slope. Until a certain level of confidence with the model is reached, some engineers may be tempted to run the model alongside other commonly used slope stability models. However, it is important to not run the model using the same soil properties since more accurate soil properties can be used if soil suction is used.

REFERENCES

Aitchison, G.H. (ed.) (1965). "Moisture Equilibria and Moisture Changes in Soils Beneath Covered Areas," *A symposium in print*. Butterworths, Sydney, Australia, 278 pp.

Anderson, M.G. and Lloyd, D.M. (1991). "Using a Combined Slope Hydrology-Stability Model to Develop Cut Slope Design Charts," *Proc. Inst. Civ. Engineers*, 91, pp. 705-718.

Bishop, D.M. and Stevens, M.E. (1964). "Landslides on Logged Areas Southeast Alaska," *Res. Pap. NOR-1, For. Serv.*, 18pp..

Bolt, G.H. and Miller, R.D. (1958). "Calculation of Total and Component Potentials of Water in Soil," *Amer. Geophys. Union Transportation*, vol. 39, pp. 917-928.

Bowles, J.E. (1995). *Foundation Analysis and Design (5th Edition)*, McGraw-Hill, 1024 pp.

Buckingham, E. (1907). "Studies of The Movement of Soil Moisture," *U.S.D.A. Bur. of Soils,* Bulletin No. 38

Burroughs, E.P. and Thomas, R.R. (1976). "Root Strength of Douglas Fir as a Factor in Slope Stability," *USDA Forest Service Review*, INT 1600-1612

Childs, E.C. and Collis-George, N. (1950). "The Permeability of Porous Materials," *Proc. Royal Soc.*, vol. 201A, pp. 392-405.

Collison, A.J.C. (1993). *Assessing the Influence of Vegetation on Slope Stability in the Tropics,* Ph.D. Thesis, University of Bristol.

Collison, A.J.C. and Anderson, M.G. (1996). "Using a Combined Slope Hydrology/Stability Model to Identify Suitable Conditions for Landslide Prevention by Vegetation in the Humid Tropics," *Earth Surface Processes and Landforms*, 21, pp. 737-747.

Collison, A.J.C.; Anderson, M.G.; and Lloyd, D.M. (1995). "Impact of Vegetation on Slope Stability in a Humid Tropical Environment: a Modeling Approach," *Proceedings of the Institute Civil Engineers, Water Maritime & Energy*, 112, pp. 168-175.

Corey, A.T. and Kemper, W.D. (1961). "Concept of Total Potential in Water and Its Limitations," *Soil Science*., vol. 91, no. 5, pp. 299-305.

Corey, A.T.; Slayter, R.O.; and Kemper, W.D. (1967). "Comparative Terminologies for Water in the Soil-Plant-Atmosphere System," in *Irrigation in Agricultural Soils*, Hagen, R.M. et al., Eds., *Amer. Soc. Agron.*, Mono, no. 11, ch. 22.

Darcy, H. (1856). *Les Fonaines Pulique de la Villa de Dijon*, Dalmont: Paris

Dragovich, J.D.; Logan, R.L.; Schasse, H.W.; Walsh, T.J.; Lingley Jr., W.S.; Norman D.K.; Gerstel, W.J.; Lapen, T.J.; Schuster, J.E.; and Myers, K.D. (2002). "Geologic Map of Washington – Northwest Quadrant," Washington Division of Geology and Earth Resources Geologic Map GM-50, 3 sheets, Scale 1:250000, 72 pp..

Edlefsen, N.E. and Anderson, A.B.C. (1943). "Thermodynamics of Soil Moisture," *Hilgardia*, vol. 15, pp. 31-298

Feddes, R.A.; Kowalik, P.; Kolinska-Malinka, K.; and Zaradny, H. (1976). "Simulation of Field Water Uptake by Plants Using a Soil Water Dependent Root Extraction Functions," *Journal of Hydrology*, 31, pp. 13-26.

Fredlund, D.G.; Morgenstern N.R.; and Widger R.A. (1978). "The Shear Strength of Saturated Soil," *Can. Geotech. J.*, 15, pp. 313-321.

Fredlund, D.G. and Rahardjo, H. (1988). "State-of-Development in the Measurement of Soil Suction," *Proc. Int. Conf. Eng. Problems on Regional Soils*, Beijing, China, pp. 582-588

Fredlund, D.G. and Rahardjo, H. (1993). "Soil Mechanics for Unsaturated Soils" John Wiley & Sons Inc. New York.

Gan, J.K-M.; Fredlund, D.G.; and Rahardjo, H. (1988). "Determination of Shear Strength Parameters of an Unsaturated Soil Using the Direct Shear Test," *Can. Geotech. J.*, 25, pp. 500-510.

Gardner, W.R. and Widtsoe J.A. (1921). "The Movement of Soil Moisture," *Soil Science*, vol. 11, pp. 215-232.

Gerstel, W.J. and Lingley, W.S. (2000). "Geologic Map of the Forks 1:100,000 Quadrangle," Washington Division of Geology and Earth Resources, Open File Report 2000-4, Plate 1, Scale 1:100000.

Gray, D.H. (1978). "Role of Woody Vegetation in Reinforcing Soils and Stabilizing Slopes," *Symposium on Soil Reinforcing and Stabilizing Techniques*, Sydney, Australia, pp. 253-306.

Griffiths, D.V. and Lu, N. (2005). "Unsaturated Slope Stability Analysis With Steady Infiltration or Evaporation Using Elasto-Plastic Finite Elements," Int. J. Numer. Anal. Geomech., 29, pp. 249-267.

Halloin, L.J.; Mofjeld, N.R.; Chadwick, O.A.; and Schmidt, W. (1987). "Soil Survey of Clallam County Area, Washington," United States Department of Agriculture, Soil Conservation Services in Cooperation with Washington State Department of Natural Resource;, Washington State University, Agriculture Research Center; and Clallam County Commissioners, pp. 137.

Hausmann, M.R. (1978). *Behavior and Analysis of Reinforced Soil*, Ph.D. Thesis, University of South Wales, Sydney, Australia.

Holtz, R.D. and Kovacs, W.D. (1981), *An Introduction to Geotechnical Engineering*, Prentice Hall, Upper Saddle River, N.J., 733 pp..

Krahn, J. and Fredlund, D.G. (1972). "On Total Matric and Osmotic Suction," *J. Soil Sci.*, vol. 114, no. 5, pp. 339-348.

Lim, T.T.; Rahardjo, H.; Chang, M.F.; and Fredlund, D.G. (1996). "Effect of Rainfall On Matric Suctions in a Residual Soil Slope," *Can. Geotech. J*., 33, pp. 618-628.

Lu, N. and Godt, J. (2008). "Infinite Slope Stability Under Steady Unsaturated Seepage Conditions," *Water Resour. Res*., 44.

Lu, N. and Likos, W.J. (2004). *Unsaturated Soil Mechanics*, 556 pp., John Wiley Hoboken, N.J..

Lu, N. and Likos, W.J. (2006). "Suction Stress Characteristic Curve for Unsaturated Soil," *J. Geotech. Geoenviron. Eng.*, 133(2), pp. 131-142.

Marshall, T.J. and Holmes, J.W. (1979). *Soil Physics*, Cambridge University Press: Cambridge.

McCreary, F.R. Raver, M.L. (1975). "Soil Survey of Jefferson County Area, Washington," United States Department of Agriculture, Soil Conservation Service in Cooperation with the Washington Agricultural Experiment Station, pp. 70.

National Oceanic and Atmospheric Administration (2009). NNDC Online Climate Data, National Environment satellite Data and Information Services. <http://hurricane/pls/plclimprod/poemain.cdobystn>

O'Loughlin, C.L. (1974). "A Study of Tree Root Strength Deterioration following Clearfelling," *Can. J. For. Res.*, 4(1), pp. 107-113.

O'Loughlin, C.L. and Zimmer, R.R. (1982). "The Importance of Root Strength and Deterioration Rates Upon Edaphic Stability in Steep-land Forests," in *Carbon Uptake and Allocation in Subalpine Ecosystems as a Key to Management: Proceedings of an IUFRO Workshop*, *Int. Union of For. Res. Organ.*, pp. 70-78.

Olson, R.E. and Langfelder, L.J. (1965). "Pore-Water Pressures in Unsaturated Soils," *J. Soil Mech. Found. Div., Proc. Amer. Soc. Civil Eng.*, vol. 91, SM4 pp. 127-160.

Pufahl, D.E. (1970). "Evaluation of Effective Stress Components in Non-Saturated Soils," *M.Sc. Thesis*, Univ, of Saskatchewan, Sakatoon, Sask., Canada, pp.88.

Richards, L.A. (1928). "The Usefulness of Capillary Potential of Soil Moisture and plant Investigators," *J. Agric. Res.*, vol. 37, pp. 719-742.

Ries III, K.G.; Guthrie, J.G.; Rea, A. H.; Steeves, P.A.; and Stewart, D.W. (2008). "Stream Stats: A Water Resources Web Application," U.S. Department of the Interior, U.S. Geological Survey, USGS Fact Sheet FS 2008-3067.

Rutter, A.J.; Kershaw, K.A.; and Robins, P.C. (1971). "A Predictive Model of Rainfall Interception in Forests. I. Derivation of the Model From Observation in Plantation of Corsican Pine," *Agricultural Meteorology*, 9, pp. 367-384.

Schofield, R. (1935). "The pF of the Water in Soil," *Trans. 3rd Int. Congress Soil Sci.*, vol. 2, pp. 37-48.

Sivakugan, N. and Das, B.M. (2010). *Geotechnical Engineering: A Problem Solving Approach*, J. Ross Publishing Co., USA, 505 pp..

Sharma, S. (1996). "Slope Stability Concepts," in *Slope Stability and Stabilization Methods*, Abramson, L.W. et al., John Wiley & Sons Inc. New York, pp.337-440.

Slaughter, S.L. (2007). "Clallam River WAU, Landslide Hazard Zonation Project, Clallam County, Washington," Forest Practices Division, 26 pp.

Slaughter, S.L. and Lingley Jr., W.S. (2006). "Mass Wasting Assessment for the State Lands Queets Block: Parts of Lower Queets River and Metheney Creek Watershed Administrative Units Jefferson and Grays Harbor Counties, Washington," Washington State Department of Natural Resources, 35 pp.

Tabor, R.W., and Cady, W.M. (1978). "Geologic Map of the Olympic Peninsula," Washington: U.S. Geological Survey Misc. Inv. map 994, scales 1:125000.

Turmanina, V.I. (1965) "The Strength of Tree Roots," Bulletin of the Moscow Society of Naturalists, Biological Section, Vol. 70, pp. 36-45

United States Dept. of Agric. Handbook No. 60. (1953). "Diagnosis and Improvement of Saline and Alkali Soils," *Government Printing Office*, Washington, D.C. pp. 7-33

U.S. Geological Survey. (2009). Landslide Hazard Program. <http://landslides.usgs.gov/>

Valene, F.; David, J.S.; and Gash, J.H.C. (1997). "Modeling Interception Loss for Two Sparse Eucalypt and Pine Forests In Central Portugal Using Reformulated Rutter and Gash Analytical Models." *Journal of Hydrology*, 190, pp 141-162.

Washington State Department of Natural Resources. (2009). Landslides. <http://www.dnr.wa.gov/ResearchScience/Topics/GeologicHazardsMapping/Pages/landslides.aspx>

Wilkinson, P.L.; Brooks, S.M.; and Anderson, M.G. (1998). "Investigating the Effect of Moisture Extraction by Vegetation upon Slope Stability: Further Developments of Combined Hydrology and Stability Model (CHASM)," *British Hydrological Society International Symposium on Hydrology in Changing Environment. Theme 4: Hydrology of Environmental Hazards*, Exeter., pp. 165-178.

Wilkinson, P.L.; Anderson, M.G.; and Lloyd, D.M. (2002). "An Integrated Hydrological Model for Rain-Induced Landslide Prediction," *Earth Surface Processes and Landforms*, 27, pp. 1285-1297.

Wieczorek, G.F. (1996). "Landslide Triggering Mechanisms," in *Landslides: Investigation and Mitigation*, Turner A.K. and Schuster R.L., National Academy Press, Washington, D.C., S.R. 247, pp. 76-90.

Wray, W.K. (1984). "The Principle of Soil suction and its Geotechnical Engineering Applications," *Proc. 5th Int. Conf. Expansive Soils*, Adelaide, South Australia, pp. 114-119.

Wu, T.H. (1976), "Investigation of Landslides on Prince of Wales Island," *Geotechnical Engineering Report 5*, Civil Engineering Department, Ohio State University, Columbus.

Wu, T.H. (1983). "Effect of Vegetation Roots on Slope Stability," *Progress Report 2*, Ohio State University, Columbus.

Wu, T.H. (1984). "Effect of Vegetation on Slope Stability," in *Soil Reinforcement and Moisture Effects on Slope Stability*, Transportation Research Record 965, pp. 37-46.

Wu, T.H.; McKinnel, W.P.; and Swanston, D.N. (1979). "Strength of Tree Roots and Landslides on Prince of Wales Island, Alaska," *Can. Geotech. J.*, 16(1), pp. 19-33.